Simvastatin inhibits PD-L1 via ILF3 to enhance CD8 + T cell-mediated ferroptosis in gastric cancer cells

Danping Sun
Qilu Hospital, Shandong University
Xiaohan Cui
Qilu Hospital, Shandong University
Wenshuo Yang
Qilu Hospital, Shandong University
Meng Wei
Qilu Hospital, Shandong University
Zhibo Yan
Qilu Hospital, Shandong University
Mingxiang Zhang
Qilu Hospital, Shandong University
Zuoyang Wang
Qilu Hospital, Shandong University
Wenbin Yu (wenbin_yu2003@163.com)
Qilu Hospital, Shandong University

Research Article

Keywords: Simvastatin, ILF3, PD-L1, HDAC6, DEPTOR/mTOR, Ferroptosis

Posted Date: January 31st, 2024

DOI: https://doi.org/10.21203/rs.3.rs-3904464/v1

Additional Declarations: No competing interests reported.

Abstract

Background

Immunotherapy is vital in the comprehensive treatment of gastric cancer (GC). However, the prognosis of GC patients remains unfavorable, necessitating to exploration of novel therapeutic approaches and medications.

Methods

PD-L1 expression was observed using small interfering RNA and plasmid to knock down and overexpress ILF3, respectively. The expression of ILF3, PD-L1, and ferroptosis marker molecules (SLC7A11 and GPX4) was detected upon simvastatin stimulation of gastric cancer cells co-cultured with activated $CD8^+$ T cells. To assess the impact of ILF3 and simvastatin stimulation on the induction of ferroptosis in gastric cancer cells by $CD8^+$ T cells, various assays including CCK8, MTT, ROS, Fe2+, MDA, GSH, and LPO were conducted. Cleavage under targets and Tagmentation (CUT&Tag) was employed to validate the mechanism of simvastatin by regulating ILF3 expression. Whole genome sequencing and KEGG analysis reveal that ILF3 regulates PD-L1 expression through the DEPTOR/mTOR signaling pathway.

Results

Statin treatment decreased the serum levels of ILF3 and PD-L1. This study found that ILF3 was positively correlated with the expression of PD-L1, and the knockdown of ILF3 effectively inhibited the expression of PD-L1, thus enhancing the cytotoxicity of $CD8^+$ T cells to gastric cancer cells. Meanwhile, simvastatin inhibited the expression of PD-L1 through ILF3, which enhanced the induction of ferroptosis in gastric cancer cells by $CD8^+$ T cells. Further studies found that simvastatin inhibited ILF3 expression by decreasing the acetylation level at residue site H3K14 in ILF3, while ILF3 inhibited PD-L1 expression through the DEPTOR/mTOR pathway.

Conclusions

Simvastatin further recruited $CD8^+$ T cells to enhance anti-tumor immunity by inhibiting PD-L1 expression by ILF3 and induced GC cells to undergo ferroptosis to achieve synergistic immunotherapy. This study elucidated the new mechanism of statins to improve GC immunotherapeutic effect. It revealed a new theoretical basis for using statins in GC treatment to improve the prognosis of GC patients.

Introduction

Gastric cancer (GC) ranks as the fifth most prevalent malignancy globally[1]. Despite implementing a comprehensive treatment approach primarily focused on surgical intervention, with chemotherapy and immunotherapy as adjunctive measures, the 5-year survival rate for patients with advanced GC remains below 30%[2, 3]. It is essential to highlight that chemotherapeutic resistance, recurrence, and distant metastases are the primary factors for GC treatment failure[4, 5]. Consequently, it is urgently needed to identify novel mechanisms and therapeutic targets for GC development.

As an inhibitor of 3-hydroxy-3-methylglutaryl coenzyme A, the statin is widely used clinically as a lipid-lowering agent and ferroptosis inducers[6, 7]. Statins can act against cancer in several ways; for example, they inhibit tumor proliferation by inhibiting cholesterol synthesis[8]. In breast cancer, simvastatin inhibits HMGCR expression and suppresses the mevalonate (MVA) pathway and GPX4 production, which induces cancer cell ferroptosis[9]. Rosuvastatin (RSV) encapsulated in silk fibroin nanoparticles named Cu-SF(RSV)NPs, which enhance breast cancer cell sensitivity to ferroptosis by inhibiting the CoQ/FSP1 axis[10]. Furthermore, statins are crucial in enhancing the effectiveness of immunotherapy of malignant tumors. Statins may synergize the clinical effects of programmed cell death protein-1 (PD-1) inhibitors to improve the prognosis of patients with malignant pleural mesothelioma and non-small cell lung cancer[11], and the administration of MVA increased programmed death ligand 1(PD-L1) expression in lung cancer cells. Moreover, rosuvastatin effectively hindered MVA-induced PD-L1 expression[12]. However, this type of studies is still insufficient in GC. Therefore, further studies are required to determine the potential of statins in enhancing the therapeutic efficacy of GC immunotherapy by inhibiting PD-L1 expression.

Interleukin enhancement-binding factor 3 (ILF3) is located on chromosome 19 and encodes a double-stranded RNA-binding protein that regulates gene expression and stabilizes mRNA levels[13, 14]. Recently, a progressive surge in the quantity of research on ILF3 elucidates its role in fostering the progression of malignant tumors via the regulation of nutrient metabolism. For example, ILF3 promotes colorectal cancer by stabilizing mRNA levels of essential genes in the Serine–Glycine–One-Carbon metabolic pathway[15]. The high expression of ILF3 promotes esophageal cancer progression by affecting glycolytic pathways leading to metabolic reprogramming[16]. Moreover, ILF3 can impede the maturation of dendritic cells and restrict innate immune responses through the regulation of lipid metabolism[17]. Recent studies have demonstrated a significant association between ILF3 expression and immune cell infiltration; for example, ILF3 exhibits a positive correlation with PD-L1 expression in hepatocellular carcinoma, and the suppression of ILF3 reduces PD-L1 expression, consequently enhancing the vulnerability of hepatocellular carcinoma to T-cell cytotoxicity[18]. A previous study found that statins inhibited ILF3 expression in GC cells. Therefore, it is necessary to investigate whether statins regulate PD-L1 expression through ILF3, thus improving the efficacy of immunotherapy.

PD-L1, also known as CD274, is a type I transmembrane immunoglobulin and is the primary ligand of PD-1[19, 20]. PD-L1 is expressed in T cells, B cells, macrophages, mast cells, vascular endothelial cells, pancreatic islet cells, and astrocytes[21]. Meanwhile, PD-L1 is elevated in various cancer tissues. The immunosuppressive receptor PD-1 is predominantly expressed in activated T cells[22]. The

immunosuppressive effects are exerted by PD-L1, which is expressed on the cancer cell surface, through its binding to the PD-1 receptor on activated T cells[23, 24]. The PD1/PD-L1 axis assumes a crucial function in facilitating the evasion of immune surveillance by malignant tumors and promoting their progression[21, 25]. Previous research has demonstrated that TRIM28 facilitates the GC advancement through suppressing PD-L1 ubiquitination, as well as activating TBKI-IRF1 and TBK1-mTOR signaling pathways, thereby augmenting the stability and expression of PD-L1[26]. An elevated PD-L1 expression is associated with the resistance to radiotherapy and chemotherapy in lung cancer patients[27]. The knockdown of HnRNPL initiates ferroptosis in prostate cancer cells by activated Jurkat cells via the suppression of PD-L1 expression; and *in vitro*, it augments the recruitment of $CD8^+$ T cells and reinforces the efficacy of anti-PD-L1 therapy[28]. Therefore, it is significantly important to identify prospective targets that regulate PD-L1 and impede its expression for enhancing immunotherapy efficacy for malignant neoplasms.

This study demonstrates a positive correlation between ILF3 and PD-L1 in GC serum and tissues, respectively; and statins effectively decrease the serum levels of PD-L1 and ILF3. Simvastatin that modulates HDAC6 overexpression reduces the acetylation at histone H3K14 site in ILF3, and decreases ILF3 expression. The down-regulation of ILF3 inhibits PD-L1 expression via the DEPTOR/mTOR pathway and facilitates activated $CD8^+$ T cells in inducing ferroptosis in GC cells. Simvastatin also synergizes the immunotherapeutic effect *in vitro* experiments by recruiting $CD8^+$ T cells to impact anti-PD-L1 immunotherapy. These findings clarify the significant contribution of simvastatin in augmenting GC immunotherapy via ILF3, which establishes a theoretical foundation for the synergistic application of statins in immunotherapeutic approaches.

Materials and Methods

Patients and tissue specimens

From January 2017 to December 2019, basic clinicopathological information, serum, GC tissue, and paracancerous tissues were collected from GC patients with radical cancer surgery at the Department of Gastrointestinal Surgery at Cheeloo College of Medicine, Shandong University (Jinan, China). All patients enrolled in the program signed an informed consent form.

Cell lines and cell culture

The GC cell lines (Ncl-N87 and HGC-27), along with the mouse forestomach carcinoma (MFC), were cultured in a medium consisting of 1640, 10% fetal bovine serum (FBS), and 1% streptomycin-penicillin antibiotic. The cells were incubated under controlled conditions (5% CO_2 and 37°C).

Transfection and sequence of small interfering RNA (siRNA)

Prior to transfection, GC cells were inoculated in a six-well plate and allowed to reach a fusion rate of 70%. Subsequently, transfection was conducted with lipofectamine RNAiMax (Invitrogen, 13778150)

reagent to introduce small interfering RNAs(siRNA) targeting various genes (Table S7). RNA extraction was performed 24h post-transfection, while protein extraction was carried out after 48h post-transfection, for subsequent experiments.

Construction and transfection of overexpression plasmids

To investigate the overexpressions of ILF3 and PD-L1 in GC cells, the genes HOMO-ILF3-C-3xFLAG and HOMO-PD-L1-C-3xFLAG were cloned into the PCDNA3.1 vector to produce PCDNA3.1-ILF3 and PCDNA3.1-PD-L1 plasmids. GC cells were cultured in six-well plates for 24 hours prior to transfection. Transfection was carried out for 24 hours with Lipofectamine 3000 (Invitrogen, L3000075) and P3000 (Invitrogen, L3000075) transfection reagents mixed with OPTI-MEM (Gibco, Shanghai, China).

Western Blot

The whole cell proteins were extracted from GC tissues and cells using RIPA lysis buffer (Beyotime, P0013B) with PMFS (Solarbio,1:1000, P0100) and protein phosphatase inhibitor (Solarbio,1:1000, P1260). Protein samples (10 μl) were separated with 10% SDS-PAGE gels and transferred to the PVDF membrane (200 mA, 90 mins). The proteins on PVDF membrane were sealed with 5% skimmed milk (1 h; room temperature), followed by an overnight incubation (4°C) with the primary antibody. Subsequently, the proteins on the PVDF membrane were incubated with either a secondary rabbit antibody or a mouse antibody (1 h; room temperature). The relative expression of proteins was detected with Amersham Imager 680 (Marlborough, USA). The primary antibodies were ILF3 (Abcam, ab92355), SLC7A11 (Abcam, ab307601), GPX4 (Abcam, ab252833), GAPDH (Abclonal, A19056), PCNA (Abcam, ab92552), HDAC1 (Abclonal, A19571), HDAC2 (Abclonal, A19626), HDAC6 (Abclonal, A3572), DEPTOR (Abclonal, A9447), mTOR (Cell Signaling Technology, 2972S), p-mTOR (CST, 5536S), H3K14ac (Abclonal, A7254), PD-L1 (Proteintech, 66248-1-Ig), CD8 (Proteintech, 66868-1-Ig), Pan acetyllysine antibody (PTM Bio, PTM-105), and 4HNE (Bioss, bs-6313R).

qRT-PCR

Total RNA from pretreated GC cells was extracted with RNAfast200 kit (Fastagen, China), and the extracted RNA was reversely transcribed into cDNA with HiScript III RT SuperMix for qPCR (R323-01, Vazyme, China), and cDNA was used to perform qRT-PCR with the ChamQ Universal SYBR qPCR Master Mix (Vazyme, China). The designed primer sequences are shown in Table S8.

IHC

IHC was performed as previously described[29]. IHC staining was performed with ILF3, DEPTOR, mTOR, 4NHE, GPX4, PD-L1, and CD8 primary antibodies. The staining results were scored with an H-score based on the percentage of positively stained cancer cells and the intensity of staining. The corresponding H-score scores were plotted on a histogram statistics.

Isolation and culture of human $CD8^+$ T cell

The venous blood was collected and peripheral blood mononuclear cells (PBMCs) were isolated using Ficoll density gradient centrifugation. The isolation and purification of $CD8^+$ T cells were performed with the Dynabeads® Untouched™ Human $CD8^+$ T Cells kit (ThermoFisher,11348D). The anti-CD3 antibody was diluted with phosphate-buffered saline (PBS) to a concentration of 5μg/ml. Subsequently, a volume (500ul) of the diluted antibody was added to each well of a six-well plate and incubated overnight at 4℃. Simultaneously, $CD8^+$ T cells were activated and cultured in complete RPMI 1640 medium, anti-CD28 antibody (5 μg/ml) and IL-2 (10 ng/ml) in each well. Alternate the fluid every 48 hours and conduct observations on the cellular condition and proliferation. GC cells were co-cultivated with activated $CD8^+$ T cells in a 1:6 ratio using six-well plates (48 h).

Cell viability assay (CCK8)

A total of 3000 GC cells and 100 μl GC medium per well were added in a 96-well plate. Different groups of GC cells were treated differently per the experimental requirements. After 24h stimulation, 10μl of detection reagent (DOJINDO, Cell Counting Kit-8, CK04) was added to each well, and the absorbance value of each well was detected at 450um after 2.5 h with an enzyme labeler.

MTT cytotoxicity detection

A total of 5×104 cells/ml suspension of GC in 100 μl were added to each 96-well plate well. After 24h stimulation with different concentrations of drugs, 10ul MTT solution (Beyotime, C0009S) was added to each well, and incubation was continued for 4 h. Each well was continued by adding 100ul of Formazan solution mixed well, and incubation was continued for 3 h. At the end of the incubation, the absorbance value of each well was measured at 570 nm with an enzyme labeler.

Calcein AM/PI cell viability Assay

After GC cells were inoculated into 12-well cell plates, various experimental treatments were applied for 24 h. Subsequently, the cells were stained with Calcein AM and propidium iodide (PI) (Beyotime, C2015M) (30 min; 37°C; dark). Finally, a fluorescence microscope was utilized to observe the green fluorescence of live cells and the red fluorescence of dead cells.

Transmission electron microscopy (TEM)

The GC cells in the pre-treated six-well plate were added with electron microscope fixative, fixed at room temperature, and protected from light for 5 min, and then the cells were gently scraped off in one direction with a cell scraper and transferred to a centrifuge tube. The GC cells precipitate was collected after centrifugation (1000 rpm/min; 5 min). After discarding the fixative and resuspending the cells with a new electron microscope fixative, the cells were fixed (room temperature; dark;30 min, and 4℃). Servicebio (Wuhan, China) conducted the TEM imaging.

Intracellular reactive oxygen species (ROS) detection

After different pre-treatments, a ROS assay kit (Beyotime, S0033S) was used to detect ROS levels in GC cells. The DCFH-DA stock solution was diluted at a ratio of 1:1000 and added to a 12-well plate, and

incubated (37°C; 30 min; dark). At the end of incubation, the ROS level was detected by washing with HBSS 3 times and then observed and photographed under a fluorescence microscope.

Intracellular Fe^{2+} detection

After different pre-treatments, a FerroOrange assay kit (Dojindo, F374) was use to detect Fe^{2+} levels in GC cells. FerroOrange solution was added to a twelve-well plate at 1 mmol/L concentration. Then the intracellular Fe^{2+} level was detected by observing and photographing under a fluorescence microscope after incubation (dark, 30 min).

Malondialdehyde (MDA) detection

A lipid oxidation (MDA) assay kit (Beyotime, S0131M) was used to detect MDA in GC cells with different pre-treatments. MDA content reflects the level of lipid oxidation. The samples to be tested and the MDA working solution were mixed and heated (100°C; 15 min), allowed to cool to room temperature, and then centrifuged (1000g; 10 min). A volume (200 ul) of the supernatant were added to a 96-well plate for measuring the absorbance value at 532nm. The amount of MDA per unit weight of protein was calculated.

Lipid peroxidation (LPO) detection

After different pre-treatments, the LPO assay kit (Dojindo, L248) was used to detect LPO levels in GC cells. After washing the pretreated GC cells once with HBSS, an appropriate amount of 10 ummol/L Liperfluo working solution was added and incubated (30 min; 37°C). The cells were washed twice more at the end of incubation. Trypsin-digested cells were collected by centrifugation and resuspended, and intracellular LPO levels were detected wih flow cytometry at 488 nm.

Immunofluorescence Assays

GC cells from each experimental group were pre-treated and subsequently fixed with a 4% formaldehyde solution. Following fixation, the cells were incubated at 37°C for 30 min in the presence of a 5% goat serum. After the incubation period, primary antibodies for ILF3 and PD-L1 were applied and allowed to incubate overnight at 4°C. The following day, a secondary antibody was added and incubated (37°C; 1 h). Nuclei were then stained using a DAPI working solution. The fluorescence microscopy was employed to detect and analyze the fluorescence intensity of ILF3 and PD-L1.

Analysis of cell death

GC cells were co-cultured with activated $CD8^+$ T cells, followed by digestion and resuspension in 1×Binding Buffer to achieve a cell concentration of 1×10^6 cells/ml. A workup for Annexin V-PI staining (BD Pharmingen™, 556547a) was prepared and combined with GC cells, which were then incubated (room temperature; dark; 15 min). The cell death was subsequently assessed using flow cytometry with a BD FACSCalibur system.

Crystal violet staining assay

Various group of GC cells were co-cultivated alongside $CD8^+$ T cells for 48h. The supernatant was eliminated, and GC cells were immobilized through the application of 4% paraformaldehyde for 15 min. After the removal of the supernatant, GC cells underwent staining using a 0.1% crystal violet solution, followed by the capture of an image.

Cut &Tag experiment

The Hyperactive Universal cut and tag Asssy kit for Illumina Pro (TD904, Vazyme, China) were used for subsequent experiments. Pre-treated GC cells were collected, ensuring 100,000 cells per sample. Incubate the collected cells with activated ConA Beads Pro for 10 min at room temperature. At the end of the incubation, discard the supernatant. After resuspending the cells again, incubate with H3K14ac primary antibody at 4°C overnight. The secondary antibody diluted at a 1:100 ratio was added using Dig-wash Buffer and set for 60 min at room temperature with rotation. Wash 3 times at the end of the incubation. Then wash 3 times after rotary incubation with pA/G-Tnp Pro at room temperature for 60 min. Diluted TTBL was then added and incubated (37°C; 60 min). Add 10% SDS and the appropriate amount of DNA Spike-in, mix well, and set at 55°C for 10 min before collecting the supernatant. Add activated DNA Extra Beads Pro to the collected supernatant and incubate for 20 min at room temperature. The supernatant was discarded after incubation with 1× B&W Buffer for 30 sec at room temperature and repeated once. The DNA Extra Beads Pro was resuspended by adding another 15 ul of ddH_2O, and the samples were subjected to PCR amplification. The PCR products were purified and sequenced on the Illumina platform.

Lentivirus production and constructing stable MFC cell lines

The lentivirus vector was successfully constructed at Nanjing Corues Biotechnology. The virus was obtained from the transfected 293T cells, after which the MFC cells were subsequently exposed to the viral supernatants for 48h. The MFC cells that underwent transfection were subjected to puromycin screening at a concentration of 2 μg/ml for 24 h, resulting in the establishment of a stable MFC cell line capable of expressing ILF3.

Animal experiments

Stable ILF3 overexpression and silencing (con-ILF3, oe-ILF3, nc-ILF3, and sh-ILF3) were established in MFC by lentivirus-mediated techniques, followed by *in vivo* experiments to study the effect of ILF3 expression on tumor growth. A subcutaneous tumor model was constructed with four-week-old C57BL/6. Twenty-four C57BL/6 were randomly divided into six groups, and each group was injected with 1×10^7 MFC cells subcutaneously in the left axilla. C57BL/6 in each group received the following treatments: nc-ILF3, sh-ILF3, nc-ILF3 + simvastatin; con-ILF3, oe-ILF3, oe-ILF3 + simvastatin, respectively. Tumor size was measured and volume calculated every 4 days, and after three weeks, tumors were taken to calculate final volume and weight, and growth curves and weight histograms were plotted, respectively.

Construct GC patient-derived xenografts (PDXs)

GC tissues exhibiting high or low expressed ILF3 were obtained from the operating room, which were submerged in DMEM culture medium and subsequently sectioned into 2mm×2mm dimensions. These sections were then inoculated into the axilla of NOG mice. Once the tumors reached a size of 1.5 cm, they were further sectioned into 2 mm × 2 mm dimensions and subsequently inoculated into the left axilla of SCID-NOD mice. Following successful growth of the tumor grafts, the corresponding drug treatment was administered.

Quantification and statistical analysis

SPSS and GraphPad Prism 8.0 were used for statistical data analysis. Experimental data were presented as mean ± SD of triple independent replicates. Unpaired two-tailed Student's t-test analyzed differences between the two groups. Multiple comparisons between groups were performed with the ANOVA test. A P-value < 0.05 was considered statistically significant.

Results

Statins enhanced sensitivity to chemotherapy in GC patients, and ILF3 as a potential target of statins.

GC patients who underwent preoperative neoadjuvant chemotherapy were divided into two groups treated with and without statins (≥ 6 months) (50 patients in each group). The Tumor Regression Grading (TRG) system (Table S1) is frequently employed to evaluate this treatment response of GC patients subjected to neoadjuvant therapies, typically chemotherapy or radiotherapy[30]. TRG grading of postoperative pathology were conducted between two groups of GC patients, which found that statins-treated groups exhibited more prominent tumor regression and were more sensitive to chemotherapy (Fig. 1A). The serum ILF3 was significantly reduced in statins-treated groups (Fig. 1B), with the basic clinical information for the two groups of GC patients (Table S2). Serum ILF3 was significantly elevated in GC patients compared to healthy people (Fig. 1C), with the basic clinical information of the two groups (Table S3). The Cancer Genome Atlas (TCGA) analysis found that the mRNA level of ILF3 was higher in GC tissues compared to normal tissues (Fig. 1D). Analysis of the clinical samples from our own hospital also found ILF3 expression was elevated in GC tissues compared to paracancerous tissues, which is consistent with the TCGA outcomes (Fig. 1E). The ILF3 expression was analyzed with hematoxylin-eosin (HE) staining between GC and paracancerous tissues (Fig. 1F) and immunohistochemistry (IHC) in different gastric cancer stages (Fig. 1G) found that ILF3 expression in advanced GC patients surpassed early GC patients (Fig. 1H). Scores 1 and 2 indicated low ILF3 expression, and scores 3 and 4 indicated high ILF3 expression. The Kaplan-Meier plotter and Gene Expression Profiling Interactive Analysis (GEPIA) analyses found that elevated ILF3 expression was associated with poorer overall survival (OS), post-progression survival (PPS), and disease-free survival (DFS) outcomes (Fig. 1I-K). Analysis of the clinical samples from our own hospital found that high ILF3 expression in GC patients had significantly a shorter survival period (Fig. 1L).

ILF3 modulated the expression of PD-L1 and regulated the killing effect of $CD8^+$ T cells on GC cells.

GC patients who underwent preoperative neoadjuvant chemotherapy and immunotherapy were divided into two groups treated with and without statins (≥ 6 months), and then tested the expression ofILF3 and PD-L1, respectively. TRG grading of postoperative pathology found that, in statins-treated group, low-ILF3 expression and low-PD-L1 expression groups exhibited more prominent tumor regression and were more sensitive to chemotherapy (Fig. 2A), with the basic clinical information for GC patients (Table S4-6). The serum PD-L1 was significantly reduced in statins-treated group (Fig. 2B). The Tumor Immune Estimation Resource (TIMER) analysis found that ILF3 was positively correlated with PD-L1 expression in GC tissues (Fig. 2C). The western blot and qRT-PCR results showed a positive correlation between the expression of ILF3 and PD-L1 at both protein and mRNA levels (Fig. 2D-F). Tumor cells released PD-L1 positive extracellular vesicle (EV) to evade the immune system[25]. The ELISA results demonstrated that si-ILF3 reduced the secretion of PD-L1 and oe-ILF3 increased the secretion of PD-L1(Fig. 2G). In addition, immunofluorescence further confirmed the positive correlation between ILF3 and PD-L1 in GC cells (Fig. 2H, Figure S1A, B). $CD8^+$ T cells were activated by co-stimulated with anti-CD3, anti-CD28 antibodies, and IL-2 (Fig. 2I). Activated $CD8^+$ T cells were co-cultured with GC cells following knockdown and overexpression of ILF3 for 48 hours, and the flow cytometry analysis showed that si-ILF3 resulted in an elevated rate of apoptosis in GC cells, whereas oe-ILF3 led to a declined rate of apoptosis (Fig. 2J). Calcein/PI staining revealed the killing effect of activated $CD8^+$ T on GC cells with fluorescence microscope, which showed that si-ILF3 enhanced the killing effect of activated $CD8^+$ T on GC cells, and oe-ILF3 played the contrary effect (Fig. 2M, N). The crystal violet staining analysis revealed that the number of viable GC cells decreased in the si-ILF3 group and the number of oe-ILF3 increased when it was co-cultured with activated $CD8^+$ T cells (Fig. 2K, L). The TIMER analysis found the elevated PD-L1 expression in multiple malignancies. Among them, the expression level of PD-L1 in GC exceeded that in normal gastric mucosal tissues (Figure S3A). Further investigation showed elevated PD-L1 was associated with poorer OS (Figure S3B). The TCGA analysis found that the mRNA level of PD-L1 was higher in GC tissues compared to normal tissues (Figure S3C). Analysis of the clinical samples from our own hospital also found PD-L1 expression was elevated in GC tissues compared to paracancerous tissues at both protein and mRNA levels (Figure S3D,3E). IHC showed the expressions of PD-L1 and CD8 in GC and paracanceerous tissues (Figure S3F).

Simvastatin inhibited PD-L1 via ILF3 and induced CD8 $^+$ T cell-dependent ferroptosis in GC cells.

Simvastatin, a lipophilic statin with enhanced lipid solubility, facilitates its permeation across cell membranes, thereby increasing the likelihood of exerting anticancer properties[31]. GC cells were divided into two groups cultured alone and with activated $CD8^+$ T cells, and then treated with different concentrations of simvastatin, respectively. The CCK8 assay demonstrated a significant decrease in the activity of GC cells in two groups with the increased concentration of simvastatin, and the IC_{50} values were 35μM and 15μM, respectively (Fig. 3A). The IC_{50} values of MTT assays were 31 μM and 18 μM, respectively (Fig. 3B). The western blot and qRT-PCR analyses revealed a concentration-dependent suppression of ILF3 expression by simvastatin at the mRNA and protein levels (Fig. 3C). Calcein/PI staining showed the number of dead GC cells was significantly increased in si-ILF3 and simvastatin-

stimulated groups compared to the nc-ILF3 group while co-culturing with activated $CD8^+$ T cells (Fig. 3D, Figure S1A, B). To investigate the potential induction of ferroptosis in GC cells by simvastatin, simvastatin stimulation of GC cells was accompanied with ferrostatin-1 (Ferr-1; a ferroptosis inhibitor) treatment, as well as Z-VAD-FMK (Z-VAD; an apoptosis inhibitor), and necrostatin-1s (Nec-1s; a necrosis inhibitor). The CCK8 analysis showed a significant increase in cell activity only when the GC cells were co-stimulated with the ferroptosis inhibitor Ferr-1 (Fig. 3E). The hTFtarget database analysis showed that the critical ferroptosis-associated molecules (SLC7A11 and GPX4) were potential targets of ILF3. Moreover, a positive correlation was found between the protein expression levels of ILF3 and SLC7A11, as well as GPX4 (Figure S2C), and the protein expressions of SLC7A11 and GPX4 were decreased after si-ILF3 and simvastatin stimulation of GC cells when co-cultured with activated $CD8^+$ T cells (Fig. 3F). A crucial characteristic of ferroptosis involves the diminishment or elimination of mitochondrial cristae, the rupture of the outer mitochondrial membrane, and its subsequent crumpling[32]. The different subgroups of GC cells were found under the electron microscope showed that mitochondria exhibited ferroptosis after the si-ILF3 and simvastatin stimulation of GC cells when co-cultured with activated $CD8^+$ T cells (Fig. 3H, I). Flow cytometry analysis showed the increase level of lipid peroxidation (LPO) in GC cells after the si-ILF3 and simvastatin stimulation of GC cells when co-cultured with activated CD8 + T cells (Fig. 3J, K). The levels of ROS and Fe^{2+} were elevated in the si-ILF3 and simvastatin stimulation of GC cells when co-cultured with activated CD8 + T cells with fluorescence microscope (Fig. 3L-O).

To verify the induction of ferroptosis in GC cells by simvastatin through the inhibition of ILF3 when co-cultured with activated $CD8^+$ T cells, the rescue experiment was conducted. The GC cells were divided into three groups: con-ILF3, oe-ILF3, and oe-ILF3 + simvastatin. The protein expressions of ILF3, SLC7A11, and GPX4 were reduced in the oe-ILF3 + simvastatin compared to oe-ILF3 group (Figure S2B). Calcein/PI staining showed the number of dead GC cells was increased in oe-ILF3 + simvastatin group compared to the oe-ILF3 group while co-culturing with activated $CD8^+$ T cells (Figure S2C). The levels of ROS and Fe^{2+} were elevated in oe-ILF3 + simvastatin group compared to the oe-ILF3 group while co-culturing with activated $CD8^+$ T cells with fluorescence microscope (Figure S2D, E). An increased MDA and decreased GSH levels were found in GC cells in oe-ILF3 + simvastatin group compared to the oe-ILF3 group while co-culturing with activated $CD8^+$ T cells (Figure S2F, G). Flow cytometry analysis showed the increase level of LPO in oe-ILF3 + simvastatin group compared to the oe-ILF3 group while co-culturing with activated $CD8^+$ T cells (Figure S2H).

Simvastatin inhibition of ILF3 regulated PD-L1 expression and enhanced the induction of ferroptosis in GC cells by activated $CD8^+$ T cells

After stimulation of GC cells with different concentrations of simvastatin, the expression of PD-L1 at the mRNA and protein levels was gradually decreased (Fig. 4A). PD-L1 overexpression at the protein and mRNA levels was confirmed with plasmid transfection (Fig. 4B).The decreased protein expressions of PD-L1, SLC7A11, and GPX4 were found in the si-ILF3 and simvastatin stimulation groups of GC cells when co-cultured with activated $CD8^+$ T cells (Fig. 4C). The increased protein expression of ILF3, PD-L1,

SLC7A11, and GPX4 were found in the simvastatin + oe-PD-L1 group compared to si-ILF3 and simvastatin stimulation groups of GC cells when co-cultured with activated $CD8^+$ T cells (Fig. 4D). CFDA-SE/PI staining showed the number of dead GC cells was decreased in the simvastatin + oe-PD-L1 group compared to si-ILF3 and simvastatin stimulation groups of GC cells when co-cultured with activated $CD8^+$ T cells (Fig. 4E, F). Flow cytometry analysis showed that simvastatin + oe-PD-L1 group had a decreased rate of apoptosis in GC cells compared to si-ILF3 and simvastatin stimulation groups of GC cells when co-cultured with activated $CD8^+$ T cells (Fig. 4G). The crystal violet staining revealed that the number of viable GC cells was increased in simvastatin + oe-PD-L1 group compared to si-ILF3 and simvastatin stimulation groups of GC cells when co-cultured with activated $CD8^+$ T cells (Fig. 4H). Previous studies demonstrated that inhibition of PD-L1 promoted $CD8^+$ T cells to induce ferroptosis in tumor cells, providing a new direction for immunotherapy of malignant tumors[33, 34]. A decreased MDA and increased GSH levels were found in GC cells in simvastatin + oe-PD-L1 group compared to si-ILF3 and simvastatin stimulation groups of GC cells when co-cultured with activated $CD8^+$ T cells (Fig. 4I, J). The levels of ROS and Fe^{2+} were decreased in simvastatin + oe-PD-L1 group compared to si-ILF3 and simvastatin stimulation groups of GC cells when co-cultured with activated $CD8^+$ T cells (Fig. 4K-N). Flow cytometry analysis showed the decreased level of LPO in simvastatin + oe-PD-L1 group compared to si-ILF3 and simvastatin stimulation groups of GC cells when co-cultured with activated $CD8^+$ T cells (Fig. 4O, P).

Simvastatin inhibited ILF3 expression by inhibiting H3K14ac, and ILF3 regulated PD-L1 expression through the DEPTOR/mTOR signaling pathway.

Swiss Target Prediction was utilized to predict potential targets of simvastatin by analysis of drug structure, which found that HDAC1, HDAC2, and HDAC6 had the potential to be targeted by simvastatin drugs. It means that simvastatin might inhibit ILF3 expression by inducing overexpression of the HDAC family and subsequently reducing ILF3 histone acetylation (Fig. 5A). The increased protein expression levels of HDAC1, HDAC2, and HDAC6 and the decreased protein expression of ILF3 were found under the stimulation of different concentration of simvastatin (Fig. 5B). Trichostatin (TSA) is a repressor of the HDAC family, leading to increased histone acetylation and promoting gene transcription[35]. Our study found the decreased protein expression levels of HDAC1, HDAC2, and HDAC6 and the increased protein expression of ILF3 under the co-stimulation of different concentration of simvastatin and TSA (Fig. 5C). Meanwhile, the total acetylation level in GC cells decreased with the increase of simvastatin concentration, and TSA could reduce the total acetylation level (Fig. 5D). Also simvastatin stimulation elevated the protein expressions of HDAC1, HDAC2, and HDAC6, but si-ILF3 did not impact HDAC1, HDAC2, and HDAC6 protein expression levels (Fig. 5E). Only the knockdown of HDAC6 resulted in an increase in ILF3 protein expression (Fig. 5F). The Cut & Tag Experiment showed an elevation in the acetylation at the H3K14 site in GC cells stimulated by simvastatin (Fig. 5G). A gradual decrease in acetylation at the H3K14 site was found in GC cells treated with varying concentrations of simvastatin (Fig. 5H). Additionally, simvastatin stimulation (20μM) in combination with different concentrations of TSA stimulation demonstrated a progressive increase in acetylation at the H3K14 site(Fig. 5I). After

knocking down HDAC1, HDAC2, and HDAC6, respectively, the acetylation of the H3K14 site was increased when HDAC6 was knocked down only (Fig. 5J). KEGG enrichment analysis was performed on the whole genome sequencing results of previous nc-ILF3 and si-ILF3, which showed that ILF3 regulated the mTOR signaling pathway (Fig. 5K). The differential genes enriched in the mTOR signaling pathway were WNT8B, CAB39, DEPTOR, PRKCB, and RNF152etc. The qRT-PCR results showed the most significant differences in DEPTOR expression between nc-ILF3 and si-ILF3 groups (Fig. 5L). DEPTOR protein expression was elevated, and the p-mTOR expression level was decreased, after the knockdown of ILF3, and the results were reversed after overexpression of ILF3 (Fig. 5M). Previous studies demonstrated that DEPTOR was a suppressor molecule of mTOR, which was further validated in GC cells[36]. Western blot showed an upregulation of p-mTOR expression when knockdown the expression of DFPTOR (Fig. 5N), and a slightly elevated levels of p-mTOR and PD-L1 (Fig. 5O), and SLC7A11 and GPX4 (Fig. 5P) were found in the group with both ILF3 and DEPTOR knockdown compared to the group with only ILF3 knockdown. The protein expressions of ILF3, p- mTOR, PD-L1, SLC7A11, and GPX4 were reduced in the oe-ILF3 + LY294002, which was the inhibitor of the mTOR signaling pathway, compared to the oe-ILF3 group (Fig. 5Q).

DEPTOR and mTOR expression levels correlate with the prognosis of GC patients.

The Gene Set Cancer Analysis (GSCA) database analysis found that the mRNA level of ILF3 was lower in GC tissues compared to normal tissues, and the mRNA level of mTOR was higher in GC tissues compared to normal tissues (Figure S4A, B). IHC results showed that DEPTOR was highly expressed in normal gastric tissues, and when ILF3 was lowly expressed, DEPTOR showed high expression levels. Meanwhile, mTOR expression was elevated in GC tissues, and when ILF3 was highly expressed, mTOR also showed high expression levels (Figure S4C). A negative regulatory relationship was found between ILF3 expression and DEPTOR, as well as a positive regulatory association of ILF3 expression with mTOR (Figure S4D, E). The Kaplan-Meier plotter showed a poor prognosis when low expression of DEPTOR and high expression of mTOR in GC patients (Figure S4F, G).

Simvastatin induced ferroptosis in GC cells by inhibiting PD-L1 expression by ILF3 to achieve therapeutic effects on GC

Mouse Forestomach Carcinoma (MFC) stably expressing ILF3 were constructed by lentivirus vector transfection (Fig. 6A). The C57BL/6 mice were randomly assigned to six distinct groups: nc-ILF3, sh-ILF3, nc-ILF3 + simvastatin, con-ILF3, oe-ILF3, and oe-ILF3 + simvastatin, which revealed that the suppression of ILF3 and the administration of simvastatin effectively impeded the proliferation of subcutaneous tumors (Fig. 6B, C). Growth curves demonstrated that overexpression of ILF3 facilitated the proliferation of subcutaneous tumors and simvastatin inhibited the proliferation of subcutaneous tumors (Fig. 6D, F). The weight of subcutaneous tumors were consistent with growth curve (Fig. 6E, G). PD-L1 protein expression was positively correlated with ILF3 expression, while simvastatin inhibited ILF3 and PD-L1 expressions (Fig. 6H). IHC analysis revealed a decrease in 4-HNE expression alongside elevated levels of

ILF3 and PD-L1, and elevated 4-HNE expression in simvastatin-treated groups with decreased ILF3 and PD-L1 expression (Fig. 6I-K).

Simvastatin inhibited ILF3 and enhanced anti-PD-L1 therapy efficacy by recruiting $CD8^+$ T cells in GC

This study investigated the expression levels of ILF3 in GC tissues obtained from radical gastric cancer surgery. Subsequently, GC tissue samples with high and low expressions of ILF3 were separately implanted into NOD/SCID mice to establish a GC patient xenograft (PDX) model (Fig. 7A). The high ILF3-expression group was administered with simvastatin treatment and simvastatin combined with anti-PD-L1 therapy, followed by weekly measurements of tumor size. After 5 weeks, the tumors were extracted to generate tumor growth curves and histograms depicting tumor weight for each group (Fig. 7B-D). Immunohistochemistry was conducted on paraffin sections of tumors from four distinct groups to assess the expression levels of ILF3, DEPTOR, mTOR, PD-L1, CD8, and 4-HNE, which revealed that the regulation of PD-L1 expression occurred via the DEPTOR/mTOR signaling pathway, facilitated by ILF3. Additionally, simvastatin demonstrated the potential to enhance the therapeutic efficacy of anti-PD-L1 treatment by suppressing PD-L1 expression through ILF3 and promoting the recruitment of $CD8^+$ T cells to induce ferroptosis in GC cells (Fig. 7E).

Discussion

Despite the development of a comprehensive treatment model incorporating surgery, chemotherapy, and immunotherapy, the prognosis of GC patients remains unfavorable[37]. Immunotherapy has emerged as a promising therapeutic approach for GC treatment, as it effectively augments the immune response against tumors[38]. Immune checkpoint inhibitors, especially PD-L1/PD-1 inhibitors, are pivotal in immunotherapy[39]. Hence, exploration of novel mechanisms regulating PD-L1 expression and identification of pharmaceutical agents modulating PD-L1 expression holds immense importance for the clinical management of GC and enhances prognostic outcomes among GC patients. Our study found that simvastatin enhanced the sensitivity of GC patients to immunotherapy, which led to further investigation of the role of simvastatin in promoting cytotoxic T-cell-mediated killing through ILF3-regulated PD-L1.

The efficacy of immunotherapy in treating tumors is influenced by various factors both in vivo and in vitro. The immune cell and metabolic status of the tumor microenvironment were significant determinants that impacted tumor immunogenicity[40]. Metabolic reprogramming is one of the characteristics of cancer cells[41, 42]. The rapid proliferation of tumor cells necessitated substantial quantities of lipids for the synthesis of cell membranes [43, 44] Thus, inhibition of lipid metabolism inhibited tumor cell growth and enhanced sensitivity to immunotherapy[45]. Screening for lipid metabolism differential genes in colorectal cancer, in which high expression of CYP19A1 was not only a prognostic risk factor for colorectal cancer patients, but also inhibited the expression of PD-L1 in colorectal cancer cells, which in turn enhanced the tumor killing ability of $CD8^+$ T cells[46]. And prior

research demonstrated that $CD8^+$ tumor-infiltrating lymphocytes (TILs) internalize ox-LDL through the CD36 receptor, thereby triggering lipid peroxidation and subsequently impairing the functionality of $CD8^+$ T cells[47]. The impact of lipid metabolism on PD-L1 expression and $CD8^+$ T cell function may have significant implications for the effectiveness of immunotherapy, thereby opening up novel avenues for further exploration in the field.

Statins are inhibitors of the MVA pathway and inhibit cholesterol synthesis[48], and are the most commonly lipid-lowering drugs in clinical practice. [49] Previous research has posited that statins may manifest their anti-tumor efficacy through two distinct mechanisms: metabolism-dependent, wherein they impede cholesterol synthesis to suppress tumor cells, and non-cholesterol-dependent, thereby exerting anti-tumor effects[50]. Cholesterol is essential to maintain intracellular homeostasis[51], and elevated cholesterol levels within tumor cells play a crucial role in enabling evasion of immune surveillance and fostering the upregulation of inhibitory immune checkpoint genes, consequently impeding the efficacy of antitumor responses[52]. The intermediate metabolisms of the mevalonate pathway, specifically farnesyl pyrophosphate and geranylgeranyl pyrophosphate, had the ability to prenylate the GTPases, thereby facilitating tumor progression[53]. Several studies have elucidated the cancer inhibitory effects of statins through metabolism-dependent pathways. Consequently, the present study aims to investigate the mechanism of action of simvastatin in the treatment of gastric cancer, specifically focusing on the non-metabolism-dependent pathway. The use of statins was found in studies of non-small cell lung cancer to enhance anti-PD-L1 /PD-1 therapy and prolong survival in NSCLC patients[54]. In addition, statins was found to improve breast cancer treatment by blocking PD-1/PD-L1 in clinical studies[55]. Therefore, it is plausible that statins could enhance the therapeutic outcomes of immunotherapy and improve the prognosis of tumor patients

ILF3 is a double-stranded RNA-binding protein and plays a role in the modulation of gene expression and the maintenance of mRNA stability[56]. Furthermore, ILF3 plays a crucial role in the pathogenesis and advancement of diverse malignant neoplasms. Nevertheless, more research is needed to investigate the correlation between ILF3 and immune cell infiltration, as well as the common immune checkpoint molecules, for example, PD-L1. Recent research revealed a positive correlation between the expression levels of ILF3 and the presence of tumor mutational burden (TMB) and microsatellite instability (MSI) in diverse malignant tumors. Furthermore, ILF3 was observed to exhibit a strong association with the infiltration of immune cells. Notably, the suppression of ILF3 was found to diminish the expression of PD-L1 and augment the susceptibility of hepatocellular carcinoma (HCC) cells, HCC cells to T cell cytotoxicity[57]. To date, there is a dearth of literature on the correlation between ILF3 and PD-L1 in GC. This study showed a positive correlation between the expression levels of ILF3 and PD-L1 in GC cells and tissues. Following co-culture with activated $CD8^+$ T cells, apoptosis levels were elevated in si-ILF3 GC cells and reduced in oe-ILF3 GC cells. Consequently, the suppression of ILF3 resulted in decreased PD-L1, thereby enhancing the cytotoxicity of activated $CD8^+$ T cells towards GC cells, which triggered an immune response and played a therapeutic role in GC, which align with the existing research on hepatocellular carcinoma. Previous research has demonstrated that simvastatin effectively impedes the proliferation,

migration, and invasive capacity of gastric cancer cells by targeting ILF3, a potential target for statins in the treatment of gastric cancer[29]. So further exploration revealed that simvastatin effectively suppressed the expression of PD-L1 through ILF3, consequently augmenting the cytotoxicity of $CD8^+$ T cells to GC cells. The aforementioned empirical findings elucidate a novel mechanism underlying the therapeutic efficacy of simvastatin in GC, thereby establishing a theoretical basis for the combined utilization of statins in GC immunotherapy.

Ferroptosis is a new form of regulated cell death (RCD), characterized by ion-dependent excess lipid peroxidation (LPO) and reactive oxygen species (ROS) production[58, 59]. Despite the significant contribution of immunotherapy in the management of malignant tumors, a considerable proportion of patients continue to exhibit unsatisfactory outcomes with the treatment. Recent investigations have increasingly highlighted the pivotal involvement of ferroptosis in the modulation of immunotherapy, thereby highlighting the potential of ferroptosis induction as a novel avenue in immunotherapy[60]. On the one hand, inducing the onset of ferroptosis in cancer cells may improve the efficacy of immunotherapy. The SLC7A11/GPX4 pathway plays a crucial role in mitigating the accumulation of lipid peroxidation and inhibiting the process of ferroptosis[61, 62]. For example, the expression of glutathione peroxidase 4 (GPX4) was inhibited by manganese molybdate nanoparticles to trigger and enhance tumor immunotherapy[63].

Prior research has demonstrated that the activation of $CD8^+$ T cells induced ferroptosis in tumor cells through the secretion of IFN-γ, thereby presenting a novel avenue for tumor treatment[33]. The inhibition of SLC7A11 expression by activated $CD8^+$ T cells can lead to ferroptosis in cancer cells to enhance the effectiveness of immunotherapy[33]. For immunotherapy, the clearance of tumor cells is accomplished by activated $CD8^+$ T cells through the utilization of the perforin-granzyme- and Fas/Fas ligand-pathways[64]. Therefore, $CD8^+$ T cells are essential to promote antitumor immunity, and enhancing their functionality is a crucial approach to enhance the effectiveness of immune checkpoint blockage therapy. In this study, simvastatin demonstrated the ability to suppress the expressions of SLC7A11/GPX4 through ILF3 to induce GC cell ferroptosis. Additionally, simvastatin augmented the cytotoxicity of activated $CD8^+$ T cells against GC cells by inhibiting PD-L1 expression through ILF3, which results in a synergistic induction of ferroptosis in GC cells by activated $CD8^+$ T cells. These results shed light on a novel mechanism through which simvastatin induced GC cell ferroptosis and enhanced the efficacy of immunotherapy. These findings offer a fresh theoretical foundation for the implementation of statin-based synergistic immunotherapy to enhance the prognosis of GC patients.

Conclusions

In summary, simvastatin exerted its effects on GC cells by modulating various molecular pathways. simvastatin reduced the acetylation of ILF3 H3K14 through the upregulation of HDAC6 expression, subsequently leading to a decrease in ILF3 expression. This downregulation of ILF3 inhibited the expression of PD-L1 via the DEPTOR/mTOR signaling pathway. Consequently, $CD8^+$ T cells were recruited

and the cytotoxicity against GC cells was enhanced. Moreover, simvastatin demonstrated a synergistic effect with immunotherapy and $CD8^+$ T cells to promote GC cell ferroptosis.

Abbreviations

GC: gastric cancer; PD-L1: programmed death ligand 1; ILF3: interleukin enhancement binding factor 3; MVA: mevalonate; PD-1: programmed cell death protein-1; TRG: tumor regression grading; IHC: immunohistochemistry; SLC7A11:solute carrier family 7 member 11; GPX4: Glutathione peroxidase 4; MDA: malondialdehyde; GSH: glutathione; ROS: reactive oxygen species; LPO: lipid peroxidation; H3K14ac: acetylation of H3 lysine 14; mTOR: mammalian target of rapamycin; p-mTOR; phosphorylated mammalian target of rapamycin; DEPTOR: DEP-domain-containing mTOR-interacting protein; HDAC1: histone deacetylase 1; HDAC2: histone deacetylase 2; HDAC6: histone deacetylase 6; TSA: trichostatin; MFC: mouse forestomach carcinoma; 4-HNE: 4-hydroxynonenal

Declarations

Acknowledgements

The authors also acknowledge Professor Mingxiang Zhang from The Key Laboratory of Cardiovascular Remodeling and Function Research, Chinese Ministry of Education, Chinese Ministry of Health and Chinese Academy of Medical Sciences, Department of Cardiology to assist in experimental design and guidance.

Authors' contributions

D. P. Sun and X. H. Cui performed most experiments and wrote the paper. W. B. Yu and M. X. Zhang designed the overall study. W. S. Yang was responsible for the staining and scoring of immunohistochemistry of clinical specimens. M. Wei and Z. B. Yan completed the collection and processing of clinical specimens. W. B. Yu supervised the experiments and revised the paper and acquired the funding. All authors read and approved the final manuscript.

Funding

This work was supported by the Horizontal project of Shandong University (No.6010121066).

Data availability statement

The datasets used and analyzed in this study are available from the corresponding author.

Declaration of interests

The authors declare that they have no conflicts of interest.

References

1. Sung H, Ferlay J, Siegel RL, Laversanne M, Soerjomataram I, Jemal A, Bray F: Global Cancer Statistics 2020: GLOBOCAN Estimates of Incidence and Mortality Worldwide for 36 Cancers in 185 Countries. CA Cancer J Clin 2021, 71:209–249.
2. Ajani JA, D'Amico TA, Almhanna K, Bentrem DJ, Chao J, Das P, Denlinger CS, Fanta P, Farjah F, Fuchs CS, et al: Gastric Cancer, Version 3.2016, NCCN Clinical Practice Guidelines in Oncology. J Natl Compr Canc Netw 2016, 14:1286–1312.
3. Allemani C, Matsuda T, Di Carlo V, Harewood R, Matz M, Niksic M, Bonaventure A, Valkov M, Johnson CJ, Esteve J, et al: Global surveillance of trends in cancer survival 2000-14 (CONCORD-3): analysis of individual records for 37 513 025 patients diagnosed with one of 18 cancers from 322 population-based registries in 71 countries. Lancet 2018, 391:1023–1075.
4. Zhang J, Huang J, Wang X, Chen W, Tang Q, Fang M, Qian Y: CMIP is oncogenic in human gastric cancer cells. Mol Med Rep 2017, 16:7277–7286.
5. Biagioni A, Skalamera I, Peri S, Schiavone N, Cianchi F, Giommoni E, Magnelli L, Papucci L: Update on gastric cancer treatments and gene therapies. Cancer Metastasis Rev 2019, 38:537–548.
6. Cholesterol Treatment Trialists C, Fulcher J, O'Connell R, Voysey M, Emberson J, Blackwell L, Mihaylova B, Simes J, Collins R, Kirby A, et al: Efficacy and safety of LDL-lowering therapy among men and women: meta-analysis of individual data from 174,000 participants in 27 randomised trials. Lancet 2015, 385:1397–1405.
7. Chen JJ, Galluzzi L: Fighting Resilient Cancers with Iron. Trends Cell Biol 2018, 28:77–78.
8. Notarnicola M, Messa C, Refolo MG, Tutino V, Miccolis A, Caruso MG: Synergic effect of eicosapentaenoic acid and lovastatin on gene expression of HMGCoA reductase and LDL receptor in cultured HepG2 cells. Lipids Health Dis 2010, 9:135.
9. Yao X, Xie R, Cao Y, Tang J, Men Y, Peng H, Yang W: Simvastatin induced ferroptosis for triple-negative breast cancer therapy. J Nanobiotechnology 2021, 19:311.
10. Yang J, Jia Z, Zhang J, Pan X, Wei Y, Ma S, Yang N, Liu Z, Shen Q: Metabolic Intervention Nanoparticles for Triple-Negative Breast Cancer Therapy via Overcoming FSP1-Mediated Ferroptosis Resistance. Adv Healthc Mater 2022, 11:e2102799.
11. Cantini L, Pecci F, Hurkmans DP, Belderbos RA, Lanese A, Copparoni C, Aerts S, Cornelissen R, Dumoulin DW, Fiordoliva I, et al: High-intensity statins are associated with improved clinical activity of PD-1 inhibitors in malignant pleural mesothelioma and advanced non-small cell lung cancer patients. Eur J Cancer 2021, 144:41–48.
12. Zhang W, Pan X, Xu Y, Guo H, Zheng M, Chen X, Wu H, Luan F, He Q, Ding L, Yang B: Mevalonate improves anti-PD-1/PD-L1 efficacy by stabilizing CD274 mRNA. Acta Pharm Sin B 2023, 13:2585–2600.
13. Shi L, Godfrey WR, Lin J, Zhao G, Kao PN: NF90 regulates inducible IL-2 gene expression in T cells. J Exp Med 2007, 204:971–977.

14. Grasso G, Kiernan R: The Polyvalent Role of NF90 in RNA Biology. Int J Mol Sci 2022, 23.
15. Li K, Wu JL, Qin B, Fan Z, Tang Q, Lu W, Zhang H, Xing F, Meng M, Zou S, et al: ILF3 is a substrate of SPOP for regulating serine biosynthesis in colorectal cancer. Cell Res 2020, 30:163–178.
16. Zang B, Wang W, Wang Y, Li P, Xia T, Liu X, Chen D, Piao HL, Qi H, Ma Y: Metabolomic Characterization Reveals ILF2 and ILF3 Affected Metabolic Adaptions in Esophageal Squamous Cell Carcinoma. Front Mol Biosci 2021, 8:721990.
17. Nazitto R, Amon LM, Mast FD, Aitchison JD, Aderem A, Johnson JS, Diercks AH: ILF3 Is a Negative Transcriptional Regulator of Innate Immune Responses and Myeloid Dendritic Cell Maturation. J Immunol 2021, 206:2949–2965.
18. Qiu J, Wu X, Luo Y, Yao Y, Zhang X, Pan B, Wang X, Tang N: Prognostic and immunotherapeutic predictive value of interleukin enhancer-binding factor 3 in hepatocellular carcinoma: Integrated bioinformatics and experimental analysis. Gene 2023, 856:147132.
19. Zamani MR, Aslani S, Salmaninejad A, Javan MR, Rezaei N: PD-1/PD-L and autoimmunity: A growing relationship. Cell Immunol 2016, 310:27–41.
20. Cha JH, Chan LC, Li CW, Hsu JL, Hung MC: Mechanisms Controlling PD-L1 Expression in Cancer. Mol Cell 2019, 76:359–370.
21. Sun C, Mezzadra R, Schumacher TN: Regulation and Function of the PD-L1 Checkpoint. Immunity 2018, 48:434–452.
22. Salas-Benito D, Conde E, Tamayo-Uria I, Mancheno U, Elizalde E, Garcia-Ros D, Aramendia JM, Muruzabal JC, Alcaide J, Guillen-Grima F, et al: The mutational load and a T-cell inflamed tumour phenotype identify ovarian cancer patients rendering tumour-reactive T cells from PD-1(+) tumour-infiltrating lymphocytes. Br J Cancer 2021, 124:1138–1149.
23. Topalian SL, Drake CG, Pardoll DM: Targeting the PD-1/B7-H1(PD-L1) pathway to activate anti-tumor immunity. Curr Opin Immunol 2012, 24:207–212.
24. Siemsen W, Halske C, Behrens HM, Kruger S, Becker-Pauly C, Rocken C: The putative pleiotropic functions of meprin beta in gastric cancer. Gastric Cancer 2023, 26:542–552.
25. Chen G, Huang AC, Zhang W, Zhang G, Wu M, Xu W, Yu Z, Yang J, Wang B, Sun H, et al: Exosomal PD-L1 contributes to immunosuppression and is associated with anti-PD-1 response. Nature 2018, 560:382–386.
26. Ma X, Jia S, Wang G, Liang M, Guo T, Du H, Li S, Li X, Huangfu L, Guo J, et al: TRIM28 promotes the escape of gastric cancer cells from immune surveillance by increasing PD-L1 abundance. Signal Transduct Target Ther 2023, 8:246.
27. Garcia-Perez BE, Perez-Torres C, Baltierra-Uribe SL, Castillo-Cruz J, Castrejon-Jimenez NS: Autophagy as a Target for Non-Immune Intrinsic Functions of Programmed Cell Death-Ligand 1 in Cancer. Int J Mol Sci 2023, 24.
28. Zhou X, Zou L, Liao H, Luo J, Yang T, Wu J, Chen W, Wu K, Cen S, Lv D, et al: Abrogation of HnRNP L enhances anti-PD-1 therapy efficacy via diminishing PD-L1 and promoting CD8(+) T cell-mediated ferroptosis in castration-resistant prostate cancer. Acta Pharm Sin B 2022, 12:692–707.

29. Sun D, Zhang M, Wei M, Wang Z, Qiao W, Liu P, Zhong X, Liang Y, Chen Y, Huang Y, Yu W: Ox-LDL-mediated ILF3 overexpression in gastric cancer progression by activating the PI3K/AKT/mTOR signaling pathway. Aging (Albany NY) 2022, 14:3887–3909.
30. Zhu J, Lian J, Xu B, Pang X, Ji S, Zhao Y, Lu H: Neoadjuvant immunotherapy for colorectal cancer: Right regimens, right patients, right directions? Front Immunol 2023, 14:1120684.
31. Tan P, Zhang C, Wei SY, Tang Z, Gao L, Yang L, Wei Q: Effect of statins type on incident prostate cancer risk: a meta-analysis and systematic review. Asian J Androl 2017, 19:666–671.
32. Xie Y, Hou W, Song X, Yu Y, Huang J, Sun X, Kang R, Tang D: Ferroptosis: process and function. Cell Death Differ 2016, 23:369–379.
33. Wang W, Green M, Choi JE, Gijon M, Kennedy PD, Johnson JK, Liao P, Lang X, Kryczek I, Sell A, et al: CD8(+) T cells regulate tumour ferroptosis during cancer immunotherapy. Nature 2019, 569:270–274.
34. Stockwell BR, Jiang X: A Physiological Function for Ferroptosis in Tumor Suppression by the Immune System. Cell Metab 2019, 30:14–15.
35. Zhang YX, Zhu YM, Yang XX, Gao FF, Chen J, Yu DY, Gao JQ, Chen ZN, Yang JS, Yan CX, Huo FQ: Phosphorylation of Neurofilament Light Chain in the VLO Is Correlated with Morphine-Induced Behavioral Sensitization in Rats. Int J Mol Sci 2023, 24.
36. Cui D, Dai X, Gong L, Chen X, Wang L, Xiong X, Zhao Y: DEPTOR is a direct p53 target that suppresses cell growth and chemosensitivity. Cell Death Dis 2020, 11:976.
37. Kim MS, Lim JS, Hyung WJ, Lee YC, Rha SY, Keum KC, Koom WS: Neoadjuvant chemoradiotherapy followed by D2 gastrectomy in locally advanced gastric cancer. World J Gastroenterol 2015, 21:2711–2718.
38. Marin-Acevedo JA, Chirila RM, Dronca RS: Immune Checkpoint Inhibitor Toxicities. Mayo Clin Proc 2019, 94:1321–1329.
39. Pardoll DM: The blockade of immune checkpoints in cancer immunotherapy. Nat Rev Cancer 2012, 12:252–264.
40. Morad G, Helmink BA, Sharma P, Wargo JA: Hallmarks of response, resistance, and toxicity to immune checkpoint blockade. Cell 2021, 184:5309–5337.
41. Hanahan D, Weinberg RA: Hallmarks of cancer: the next generation. Cell 2011, 144:646–674.
42. Reznik E, Luna A, Aksoy BA, Liu EM, La K, Ostrovnaya I, Creighton CJ, Hakimi AA, Sander C: A Landscape of Metabolic Variation across Tumor Types. Cell Syst 2018, 6:301–313 e303.
43. Santos CR, Schulze A: Lipid metabolism in cancer. FEBS J 2012, 279:2610–2623.
44. Liu Q, Luo Q, Halim A, Song G: Targeting lipid metabolism of cancer cells: A promising therapeutic strategy for cancer. Cancer Lett 2017, 401:39–45.
45. Gottfried E, Kreutz M, Mackensen A: Tumor metabolism as modulator of immune response and tumor progression. Semin Cancer Biol 2012, 22:335–341.

46. Liu L, Mo M, Chen X, Chao D, Zhang Y, Chen X, Wang Y, Zhang N, He N, Yuan X, et al: Targeting inhibition of prognosis-related lipid metabolism genes including CYP19A1 enhances immunotherapeutic response in colon cancer. J Exp Clin Cancer Res 2023, 42:85.
47. Xu S, Chaudhary O, Rodriguez-Morales P, Sun X, Chen D, Zappasodi R, Xu Z, Pinto AFM, Williams A, Schulze I, et al: Uptake of oxidized lipids by the scavenger receptor CD36 promotes lipid peroxidation and dysfunction in CD8(+) T cells in tumors. Immunity 2021, 54:1561–1577 e1567.
48. Zaky MY, Fan C, Zhang H, Sun XF: Unraveling the Anticancer Potential of Statins: Mechanisms and Clinical Significance. Cancers (Basel) 2023, 15.
49. Goldstein JL, Brown MS: Regulation of the mevalonate pathway. Nature 1990, 343:425–430.
50. Wang T, Seah S, Loh X, Chan CW, Hartman M, Goh BC, Lee SC: Simvastatin-induced breast cancer cell death and deactivation of PI3K/Akt and MAPK/ERK signalling are reversed by metabolic products of the mevalonate pathway. Oncotarget 2016, 7:2532–2544.
51. Espinosa G, Lopez-Montero I, Monroy F, Langevin D: Shear rheology of lipid monolayers and insights on membrane fluidity. Proc Natl Acad Sci U S A 2011, 108:6008–6013.
52. Xiao M, Xu J, Wang W, Zhang B, Liu J, Li J, Xu H, Zhao Y, Yu X, Shi S: Functional significance of cholesterol metabolism in cancer: from threat to treatment. Exp Mol Med 2023, 55:1982–1995.
53. Waller DD, Park J, Tsantrizos YS: Inhibition of farnesyl pyrophosphate (FPP) and/or geranylgeranyl pyrophosphate (GGPP) biosynthesis and its implication in the treatment of cancers. Crit Rev Biochem Mol Biol 2019, 54:41–60.
54. Mao W, Cai Y, Chen D, Jiang G, Xu Y, Chen R, Wang F, Wang X, Zheng M, Zhao X, Mei J: Statin shapes inflamed tumor microenvironment and enhances immune checkpoint blockade in non-small cell lung cancer. JCI Insight 2022, 7.
55. Choe EJ, Lee CH, Bae JH, Park JM, Park SS, Baek MC: Atorvastatin Enhances the Efficacy of Immune Checkpoint Therapy and Suppresses the Cellular and Extracellular Vesicle PD-L1. Pharmaceutics 2022, 14.
56. Castella S, Bernard R, Corno M, Fradin A, Larcher JC: Ilf3 and NF90 functions in RNA biology. Wiley Interdiscip Rev RNA 2015, 6:243–256.
57. Wang X, Liang C, Yao X, Yang RH, Zhang ZS, Liu FY, Li WQ, Pei SH, Ma J, Xie SQ, Fang D: PKM2-Induced the Phosphorylation of Histone H3 Contributes to EGF-Mediated PD-L1 Transcription in HCC. Front Pharmacol 2020, 11:577108.
58. Yang J, Ma S, Xu R, Wei Y, Zhang J, Zuo T, Wang Z, Deng H, Yang N, Shen Q: Smart biomimetic metal organic frameworks based on ROS-ferroptosis-glycolysis regulation for enhanced tumor chemo-immunotherapy. J Control Release 2021, 334:21–33.
59. Li K, Lin C, Li M, Xu K, He Y, Mao Y, Lu L, Geng W, Li X, Luo Z, Cai K: Multienzyme-like Reactivity Cooperatively Impairs Glutathione Peroxidase 4 and Ferroptosis Suppressor Protein 1 Pathways in Triple-Negative Breast Cancer for Sensitized Ferroptosis Therapy. ACS Nano 2022, 16:2381–2398.
60. Yan F, Mao C, Leung EL, Luo L: Editorial: Progress of programmed cell death in antitumor immunity. Front Immunol 2023, 14:1230490.

61. Yang WS, SriRamaratnam R, Welsch ME, Shimada K, Skouta R, Viswanathan VS, Cheah JH, Clemons PA, Shamji AF, Clish CB, et al: Regulation of ferroptotic cancer cell death by GPX4. Cell 2014, 156:317–331.
62. Lei G, Zhang Y, Koppula P, Liu X, Zhang J, Lin SH, Ajani JA, Xiao Q, Liao Z, Wang H, Gan B: The role of ferroptosis in ionizing radiation-induced cell death and tumor suppression. Cell Res 2020, 30:146–162.
63. Lei H, Li Q, Pei Z, Liu L, Yang N, Cheng L: Nonferrous Ferroptosis Inducer Manganese Molybdate Nanoparticles to Enhance Tumor Immunotherapy. Small 2023, 19:e2303438.
64. Golstein P, Griffiths GM: An early history of T cell-mediated cytotoxicity. Nat Rev Immunol 2018, 18:527–535.

Figures

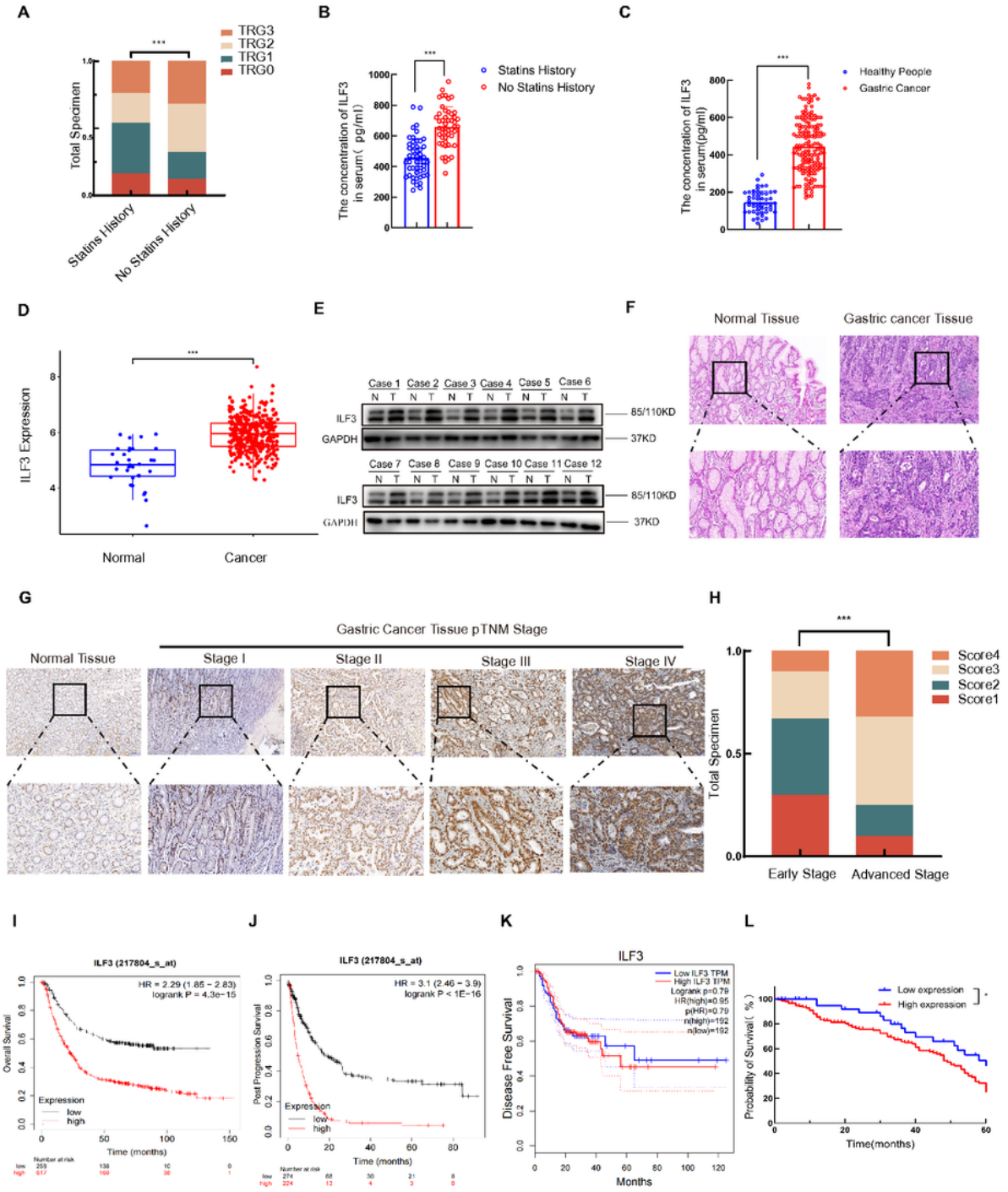

Figure 1

Statins improve chemotherapy resistance in gastric cancer patients, and ILF3 as a potential target of statins. **(a)**TRG-graded histogram of preoperative neoadjuvant gastric cancer patients with or without a history of statin use. **(b)**Serum levels of ILF3 in gastric cancer patients with a history of statin use and in gastric cancer patients without a history of statin use. **(c)**Serum levels of ILF3 in the healthy people and gastric cancer patients. **(d)**Differences in ILF3 mRNA levels between gastric cancer and normal gastric

tissues in the TCGA database. **(e)**Western blot detection the differential expression of ILF3 protein levels in gastric cancer and normal gastric tissues. **(f)**HE staining of normal gastric and gastric cancer tissues. **(g)**Detection of ILF3 expression level in normal gastric tissues and tissues with different stages of gastric cancer by immunohistochemical staining. **(h)**Statistical analysis of histograms for H score. **(i)**Relationship between ILF3 expression and overall survival rate of gastric cancer patients from the Kaplan Meier plotter. **(j)**Relationship between ILF3 expression and post-progression survival rate of gastric cancer patients from the Kaplan Meier plotter. **(k)**Relationship between ILF3 expression and disease-free survival rate of gastric cancer patients from GEPIA. **(l)**Probability of survival of gastric cancer patients with low and high ILF3 expression levels.

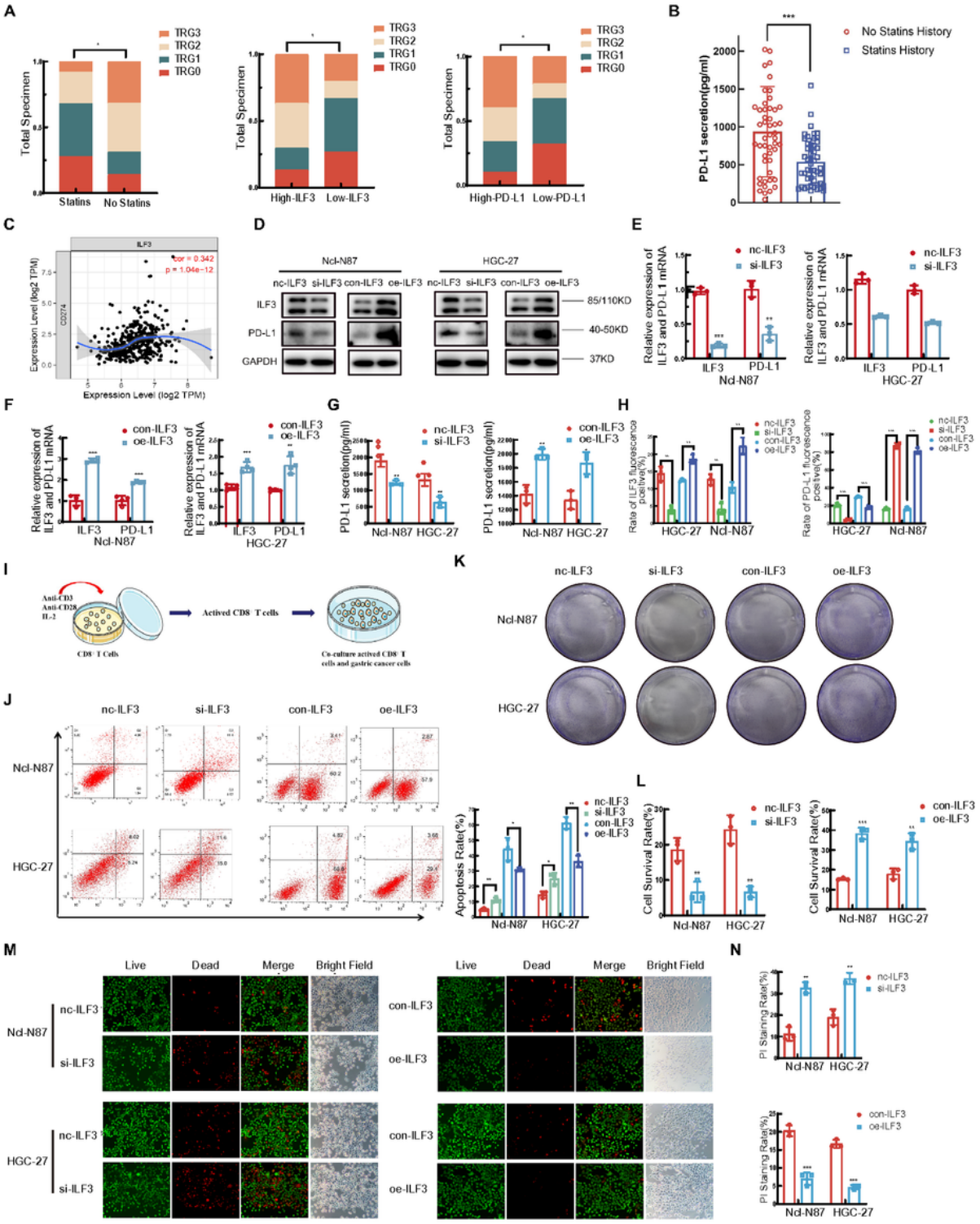

Figure 2

ILF3 modulated the expression of PD-L1 and regulated the killing of $CD8^+$ T cells to gastric cancer cells. **(a)**Association of statins history, high and low expression of ILF3 and high and low expression of PD-L1 with TRG grading in gastric cancer patients treated with preoperative neoadjuvant chemotherapy combined with immunotherapy. **(b)**Serum levels of PD-L1 in gastric cancer patients with or without a history of statin use and in gastric cancer patients treated with preoperative neoadjuvant chemotherapy

combined with immunotherapy. **(c)**Correlation between ILF3 and PD-L1 expression in gastric cancer tissues by the public database TTMER. **(d)** Western blot detection the protein level of ILF3 and PD-L1 following ILF3 knockdown and overexpression. **(e)**qRT-PCR detection the mRNA level of ILF3 and PD-L1 following ILF3 knockdown. **(f)**qRT-PCR detection the mRNA level of ILF3 and PD-L1 following ILF3 overexpression. **(g)**ELISA measured secreted PD-L1 after knockdown and overexpression of ILF3. **(h)**Immunofluorescence analyzed the expression of ILF3 and PD-L1 following ILF3 inhibition and overexpression. **(i)**Schematic diagram of activated $CD8^+$ T cells. **(j)** Effect of cell flow assay on apoptosis of gastric cancer cells co-cultured with activated $CD8^+$ T cells after knockdown and overexpression of ILF3. **(k)**Crystal violet staining the surviving gastric cancer cells co-cultured with active $CD8^+$ T cells knocking down and overexpressing ILF3. **(l)**Histogram of cell survival rate of gastric cancer cells co-cultured with activated $CD8^+$ T cells after knockdown and overexpression of ILF3. **(m)**Calcein/PI staining showed killing effect of activated $CD8^+$ T cells on gastric cancer cells after knockdown and overexpression of ILF3. **(n)** Histogram of PI staining positive rate of gastric cancer cells co-cultured with activated $CD8^+$ T cells after knockdown and overexpression of ILF3.

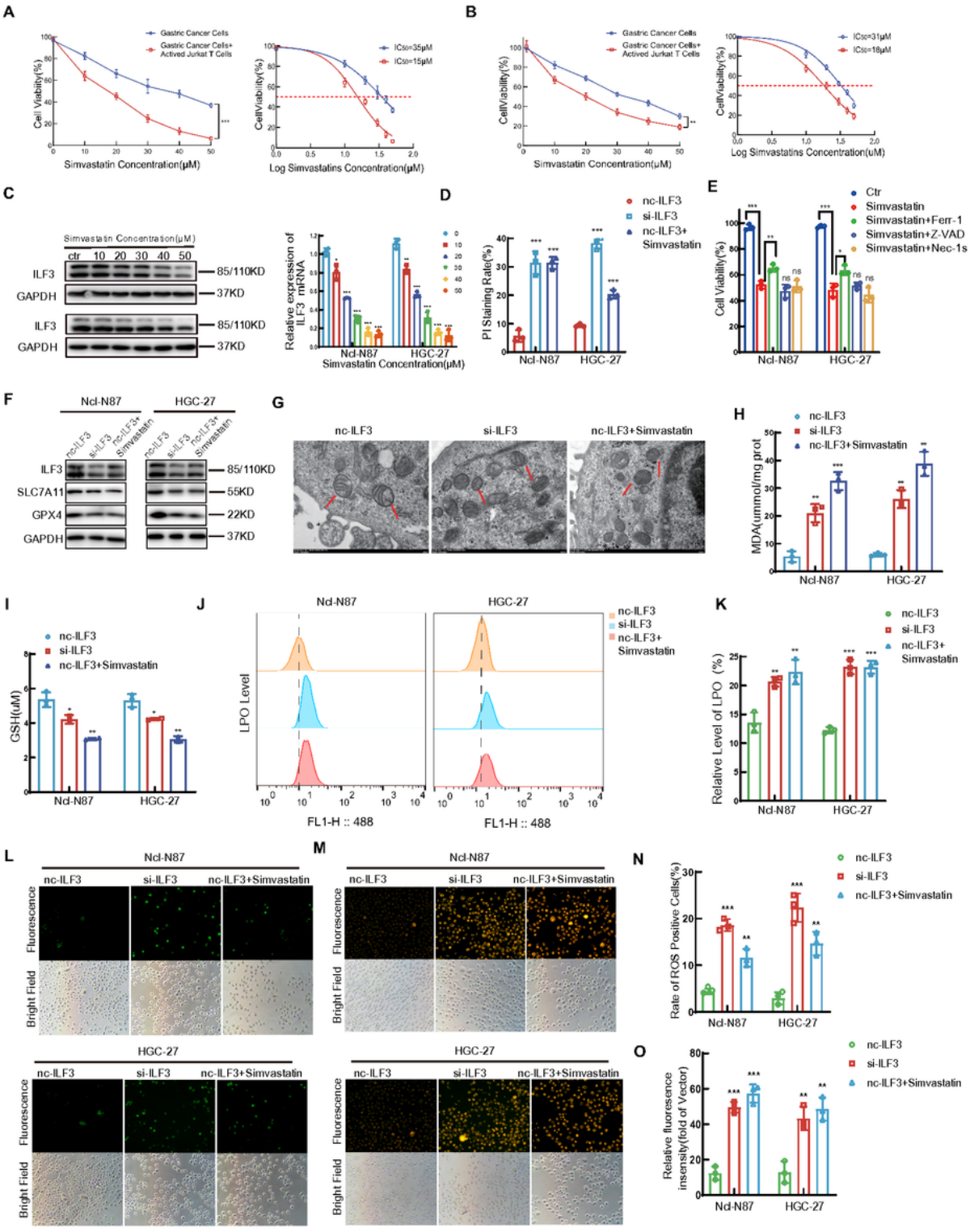

Figure 3

Simvastatin inhibited PD-L1 via ILF3 and induced $CD8^+$ T cell-dependent ferroptosis in gastric cancer cells. **(a)** CCK8 assay of cell activity and IC_{50} of gastric cancer cells after simvastatin stimulation at different concentrations when cultured alone and co-cultured with activated $CD8^+$ T cells. **(b)** MTT assay of cell activity and IC_{50} of gastric cancer cells after simvastatin stimulation at different concentrations

when cultured alone and co-cultured with activated $CD8^+$ T cells. **(c)**Western blot and qRT-PCR detection of ILF3 expression levels in gastric cancer cells after simvastatin stimulation at different concentrations. **(d)** Histogram of PI staining positive rate of gastric cancer cells in in groups of gastric cancer cells, nc-ILF3, si-ILF3, nc-ILF3+simvastatin when co-cultured with activated $CD8^+$ T cells. **(e)**Simultaneous use of ferrostatin-1 (Ferr-1), an inhibitor of ferroptosis, Z-VAD-FMK (Z-VAD), an inhibitor of apoptosis, and necroptosis inhibitor necroptin-1s (Nec-1s) based on simvastatin stimulation of gastric cancer cells were examined for gastric cancer cell activity by CCK8 assay. **(f)**Western blot detection of ILF3, SLC7A11 and GPX4 expression levels in three groups of gastric cancer cells, nc-ILF3, si-ILF3, and nc-ILF3+simvastatin when co-cultured with activated $CD8^+$ T cells.**(g)**Morphology of mitochondria in three groups of gastric cancer cells, nc-ILF3, si-ILF3, and nc-ILF3+simvastatin, observed by electron microscopy.**(h)**Detection of MDA levels in three groups of gastric cancer cells, nc-ILF3, si-ILF3, and nc-ILF3+simvastatin when co-cultured with activated $CD8^+$ T cells. **(i)**Detection of GSH levels in three groups of gastric cancer cells, nc-ILF3, si-ILF3, and nc-ILF3+simvastatin when co-cultured with activated $CD8^+$ T cells. **(j)**Cell flow assay detection of lipid peroxides levels in three groups of gastric cancer cells, nc-ILF3, si-ILF3, and nc-ILF3+simvastatin when co-cultured with activated $CD8^+$ T cells. **(k)** Histogram of relative levels of lipid peroxides in different groups of gastric cancer cells co-cultured with activated $CD8^+$ T cells. **(l)**Detection of ROS levels in the groups of gastric cancer cells co-cultured with activated $CD8^+$ T cells, nc-ILF3, si-ILF3, and nc-ILF3+simvastatin. **(m)** Detection of Fe^{2+} levels in three groups of gastric cancer cells co-cultured with activated $CD8^+$ T cells, nc-ILF3, si-ILF3, and nc-ILF3+simvastatin. **(n)** Histogram of ROS positive gastric cancer cells in in the groups of gastric cancer cells co-cultured with activated $CD8^+$ T cells, nc-ILF3, si-ILF3, and nc-ILF3+simvastatin. **(o)** Histogram of fluorescence insensity of Fe^{2+} positive gastric cancer cells in different groups.

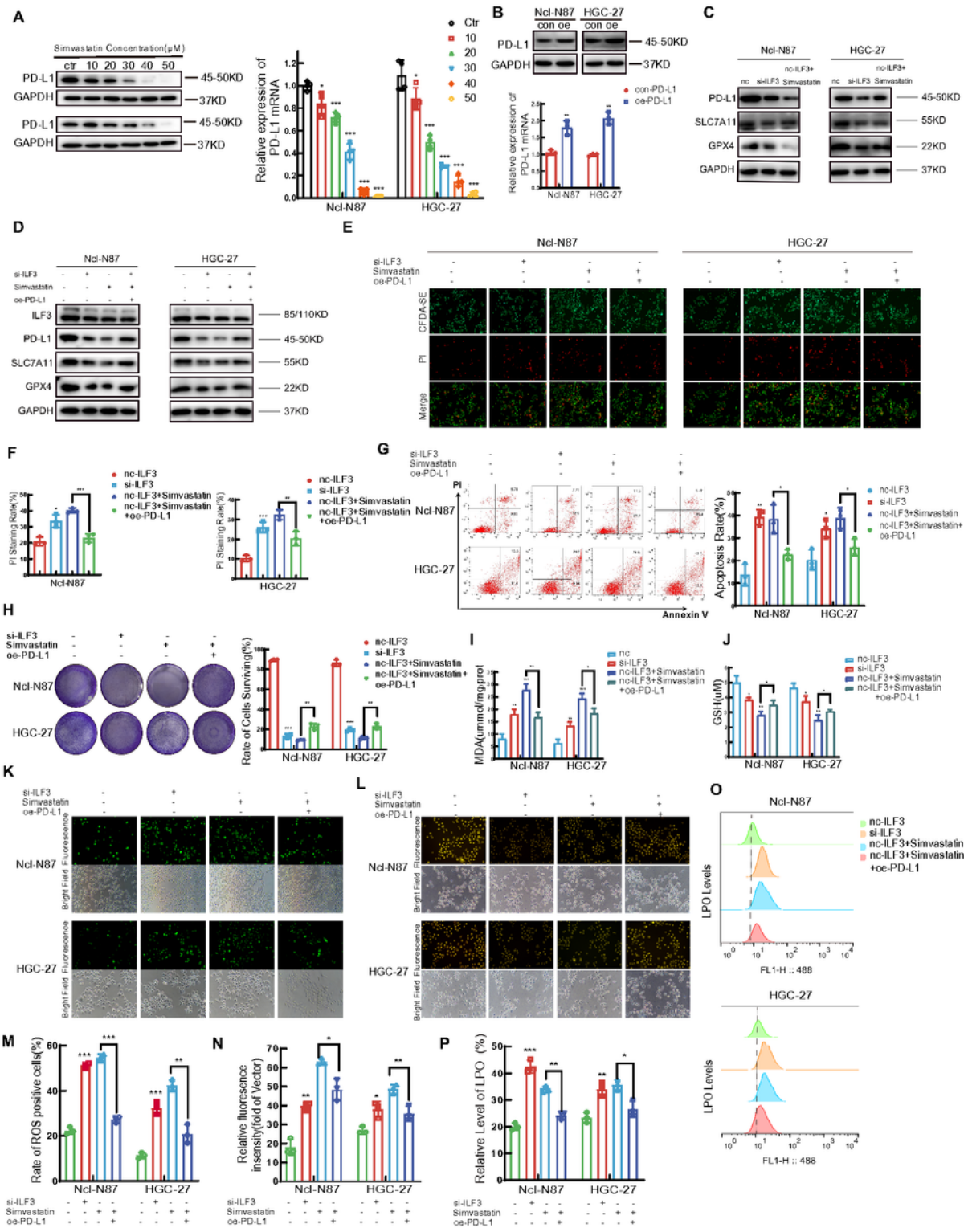

Figure 4

Simvastatin inhibition of ILF3 regulated PD-L1 expression and enhanced the induction of ferroptosis in gastric cancer cells by activated $CD8^+$ T cells. **(a)**Western blot and qRT-PCR detection of PD-L1 expression levels in gastric cancer cells after simvastatin stimulation at different concentrations. **(b)**Plasmid overexpression of PD-L1 was detected by western blot and qRT-PCR. **(c)**Western blot detection of ILF3, PD-L1, SLC7A11 and GPX4 expression after knockdown of ILF3 and simvastatin stimulation. **(d)**Western

blot detection of ILF3, PD-L1, SLC7A11 and GPX4 expression after knockdown of ILF3 and simvastatin stimulation in groups of gastric cancer cells, nc-ILF3, si-ILF3, nc-ILF3+simvastatin and nc-ILF3+simvastatin+oe-PD-L1. **(e)** CFDA-SE/PI staining showed killing effect of activated $CD8^+$ T cells on gastric cancer cells in groups of gastric cancer cells, nc-ILF3, si-ILF3, nc-ILF3+simvastatin and nc-ILF3+simvastatin+oe-PD-L1. **(f)** Histogram of PI staining positive rate of gastric cancer cells co-cultured with activated $CD8^+$ T cells in groups of nc-ILF3, si-ILF3, nc-ILF3+simvastatin and nc-ILF3+simvastatin+oe-PD-L1. **(g)**The apoptosis rate of different groups of gastric cancer cells co-cultured with activated $CD8^+$ T cells detected by cell flow assay. **(h)** Crystal violet staining the surviving gastric cancer cells co-cultured activated $CD8^+$ T cells in groups of nc-ILF3, si-ILF3, nc-ILF3+simvastatin and nc-ILF3+simvastatin+oe-PD-L1. **(i)**The level of MDA of different groups of gastric cancer cells co-cultured with activated $CD8^+$ T cells. **(j)**The level of GSH of different groups of gastric cancer cells co-cultured with activated $CD8^+$ T cells. **(k)**The level of ROS of different groups of gastric cancer cells co-cultured with activated $CD8^+$ T cells detected by fluorescence microscope. **(l)**The level of Fe^{2+} of different groups of gastric cancer cells co-cultured with activated $CD8^+$ T cells detected by fluorescence microscope. **(m)** Histogram of ROS positive gastric cancer cells in different groups. **(n)** Histogram of fluorescence insensity of Fe^{2+} positive gastric cancer cells in different groups. **(o)**Cell flow assay detection of lipid peroxides levels in different groups of gastric cancer cells co-cultured with activated $CD8^+$ T cells. **(p)** Histogram of relative levels of LPO in different groups of gastric cancer cells co-cultured with activated $CD8^+$ T cells.

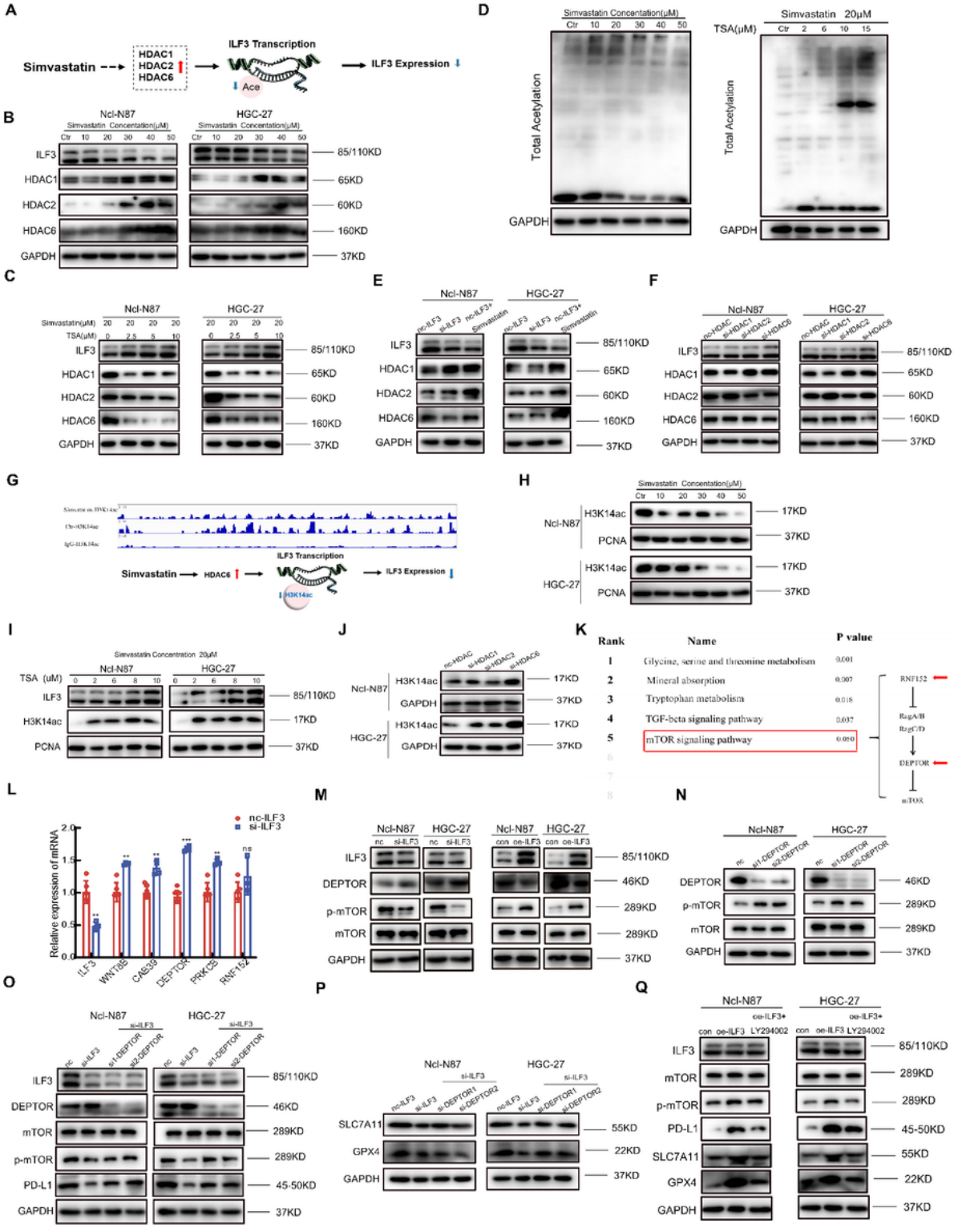

Figure 5

Simvastatin inhibited ILF3 expression by inhibiting the level of H3K14ac, and ILF3 regulated PD-L1 expression through the DEPTOR/mTOR signaling pathway. (**a**)Model of the potential mechanism by which simvastatin regulated ILF3 expression. (**b**) Western blot analysis of ILF3, HDAC1, HDAC2, and HDAC6 in gastric cancer cells after stimulation with different concentrations of simvastatin. (**c**) Western blot analysis of ILF3, HDAC1, HDAC2, and HDAC6 after co-stimulation of gastric cancer cells with

simvastatin and TSA. (**d**)Levels of total acetylation after stimulation of gastric cancer cells with different concentrations of simvastatin, and levels of total acetylation after co-stimulation of gastric cancer cells with simvastatin and TSA. (**e**) Western blot analysis of ILF3 HDAC1 HDAC2, and HDAC6 expression levels in three groups of gastric cancer cells, nc-ILF3, si-ILF3, and nc-ILF3+simvastatin.(**f**)Western blot detection of ILF3, HDAC1, HDAC2, and HDAC6 expression after knockdown of HDAC1, HDAC2, and HDAC6, respectively, using small interferences RNAs. (**g**)Results of Cut&Tag experiments and the mechanism of inhibition of ILF3 expression by simvastatin are plotted. (**h**)Western blot detection of acetylation level of H3K14 site after stimulation of gastric cancer cells with different concentrations of simvastatin. (**i**)Western blot detection of acetylation level of H3K14 site after co-stimulation of gastric cancer cells with different concentrations of simvastatin and TSA. (**j**)Western blot detection of acetylation levels of H3K14 site after knockdown of HDAC1, HDAC2, and HDAC6 using small interferences, respectively. (**k**)Results of KEGG enrichment analysis after whole gene transcriptome sequencing. (**l**)RT-qPCR detection of mRNA expression levels of WNT8B, CAB39, DEPTOR, PRKCB, and RNF152 in two groups of gastric cancer cells, nc-ILF3 and si-ILF3. **(m)**Western blot detection of ILF3, DEPTOR, mTOR, and p-mTOR expression in four groups of gastric cancer cells, nc-ILF3, si-ILF3, con-ILF3 and oe-ILF3. **(n)** Western blot detection of DEPTOR, mTOR, and p-mTOR expression levels in gastric cancer cells in three groups of gastric cancer cells, nc-DEPTOR, si-DEPTOR1, and si-DEPTOR2.**(o)**Based on knocking down ILF3 expression, DEPTOR was also knocked down with small interference, western blot detection of ILF3, DEPTOR, mTOR, p-mTOR and PD-L1 expression levels in gastric cancer cells.(**p**) Based on knocking down ILF3 expression, DEPTOR was also knocked down with small interference, western blot detection of SLC7A11, and GPX4 expression.**(q)**Western blot detection of ILF3, mTOR, p-mTOR, PD-L1, SLC7A11, and GPX4 expression levels in gastric cancer cells in three groups of gastric cancer cells, con-ILF3, oe-ILF3 and oe-ILF3+LY294002.

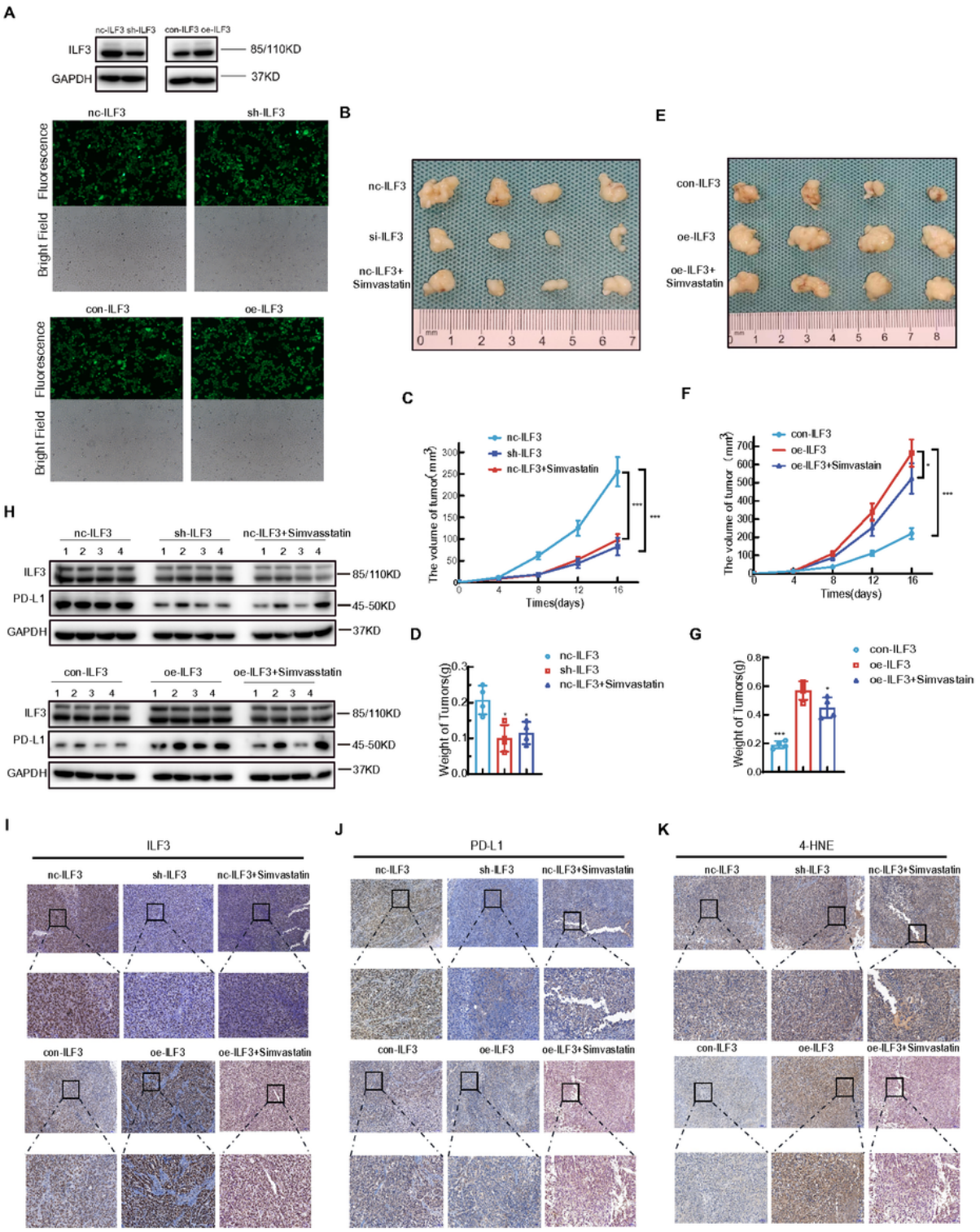

Figure 6

Simvastatin induced ferroptosis in gastric cancer cells by inhibiting PD-L1 expression by ILF3 to achieve therapeutic effect on gastric cancer. **(a)** Lentiviral construction of stably expressed MFCnc-ILF3, sh-ILF3, con-ILF3, and oe-ILF3. **(b)**Photographs and size of tumors in groups: nc-ILF3, sh-ILF3, nc-ILF3+simvastatin. **(c)**Growth curves of tumors in nc-ILF3, sh-ILF3, nc-ILF3+simvastatin groups. **(d)** Histogram of tumor weight in nc-ILF3, sh-ILF3, nc-ILF3+simvastatin groups. **(e)**Photographs and size of

tumors in groups: con-ILF3, oe-ILF3, oe-ILF3+simvastatin. **(f)**Growth curves of tumors in con-ILF3, oe-ILF3, oe-ILF3+simvastatin groups. **(g)**Histogram of tumor weight in con-ILF3, oe-ILF3, oe-ILF3+simvastatin groups. **(h)**Western blot analysis of ILF3 and PD-L1 innc-ILF3, sh-ILF3, nc-ILF3+simvastatin, con-ILF3, oe-ILF3, oe-ILF3+simvastatin groups. **(i)** IHC staining of ILF3 in different treatment groups. **(j)** IHC staining of PD-L1 in different treatment groups. **(k)** IHC staining of 4-HNE in different treatment groups.

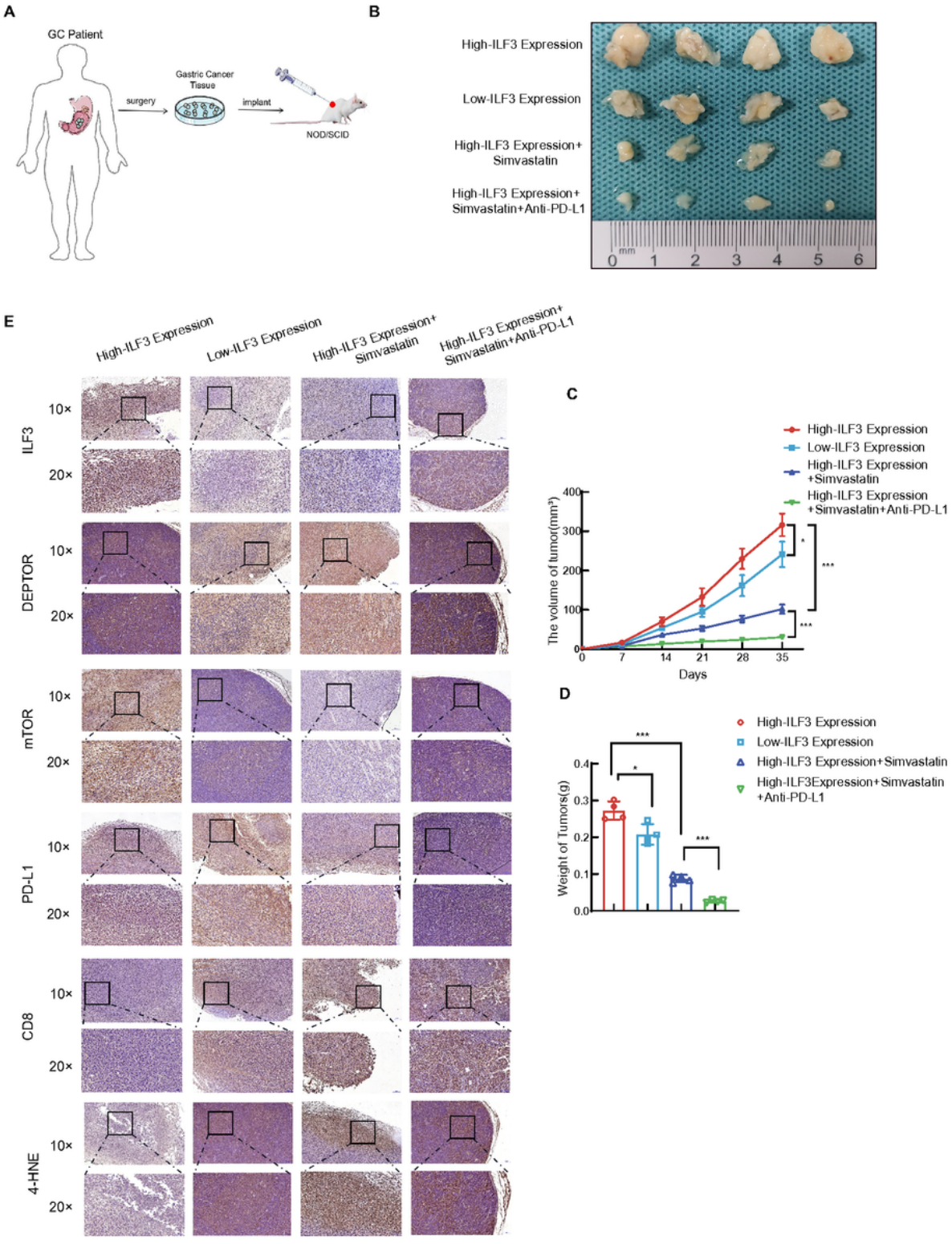

Figure 7

Simvastatin inhibited ILF3 and enhanced anti-PD-L1 therapy efficacy by recruiting $CD8^+$ T cells in gastric cancer. **(a)** Schematic diagram for constructing a PDX model. **(b)** Photographs and size of tumors in different treatment groups. **(c)** Growth curves of tumors in different treatment groups. **(d)** Histogram of tumor weight in different treatment groups. **(e)** Immunohistochemical staining for ILF3, DEPTOR, mTOR, p-mTOR, PD-L1, CD8, and 4-HNE in different treatment groups.

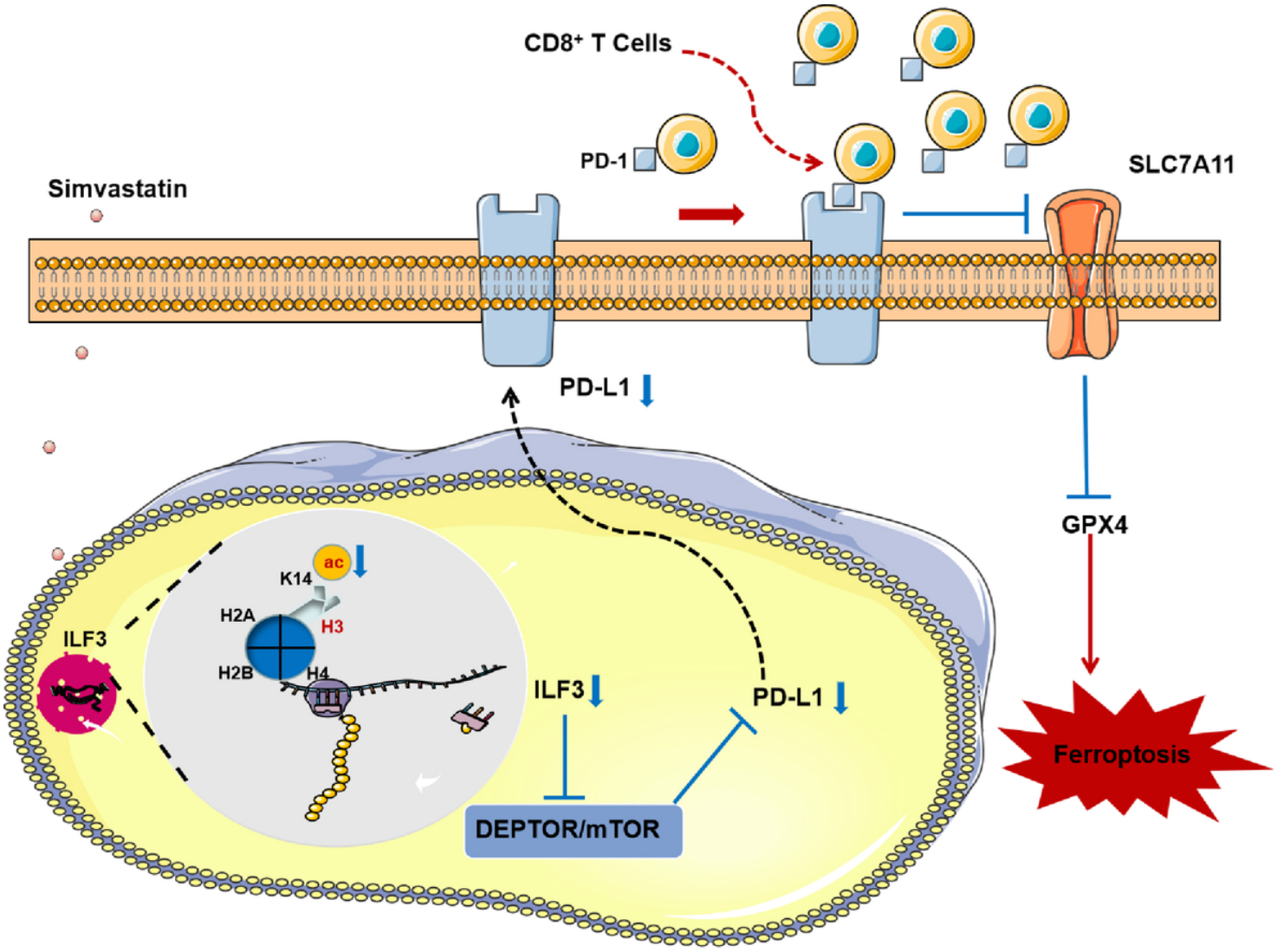

Figure 8

Legend not included with this version.

Supplementary Files

This is a list of supplementary files associated with this preprint. Click to download.

- SupplementalFigure1.pdf
- SupplementalFigure2.pdf

- SupplementalFigure3.pdf
- SupplementalFigure4.pdf
- SupplementalTable.pdf